

Oscillatory spacelike singularities: The Bianchi type $VI_{-1/9}$ vacuum models

Phillipo Lappicy* and Claes Uggla**

arXiv:2410.10375v1 [gr-qc] 14 Oct 2024

*

Departamento de Análisis Matemático y Matemática Aplicada
Universidad Complutense de Madrid
28040, Madrid, Spain
philemos@ucm.es

**

Department of Physics
Karlstad University
S-65188 Karlstad, Sweden
claes.uggla@kau.se

Abstract

The Bianchi type $VI_{-1/9}$, VIII and IX vacuum models all have 4-dimensional Hubble-normalized state spaces and are expected to have a generic initial oscillatory singularity, but the invariant boundary sets responsible for the oscillations are much more complicated for type $VI_{-1/9}$ than those of type VIII and IX. For the first time, we explicitly solve the equations on these type $VI_{-1/9}$ boundary sets and also introduce a new graphic representation of the associated network of heteroclinic chains (i.e. sequences of solutions describing the oscillations). In particular, we give examples of networks of entangled cyclic heteroclinic chains and show that only some of these cyclic heteroclinic chains are asymptotically relevant.

Contents

1. Introduction	2
2. The dynamical system and its stratification of invariant sets	4
2.1. Sets of fixed points	6
2.2. The Kasner subset \mathcal{K}	10
2.3. The Bianchi type II subset \mathcal{B}_{II}	12
2.4. The orthogonally transitive subset \mathcal{OT}	14
2.5. The hypersurface orthogonal subset \mathcal{HO}	15
2.6. The $\mathcal{W}^s(\text{PW}^\pm)$ subset	17
3. Induced discrete dynamics	17
3.1. Kasner circle transition maps	19
3.2. Frame-invariant discrete dynamics	20
3.3. From frame-invariant Kasner sequences to networks of heteroclinic chains	24
4. Examples of networks of cyclic heteroclinic chains	30
4.1. The golden ratio $u_0 = \frac{1+\sqrt{5}}{2}$	30
4.2. The silver ratio $u_0 = 1 + \sqrt{2}$	33
4.3. The alloy ratio $u_0 = 1 + \sqrt{3}$	35
4.4. Comparisons between networks of type $VI_{-1/9}$ and type VIII, IX	38
A. Dynamics in invariant subsets	40
A.1. A toy model	40
A.2. The Kasner subset \mathcal{K}	42
A.3. The Bianchi type II subset \mathcal{B}_{II}	43
A.4. The \mathcal{HO} subset	46

1. Introduction

An important feature of Einstein’s field equations is that they result in space-time singularities under quite general conditions, as shown by the Penrose-Hawking singularity theorems and variations thereof, see e.g. [49, 20, 16, 19, 58]. These theorems, however, say little about the nature of generic space-time singularities.

To make mathematically rigorous progress about this issue, one has to make more stringent conditions on the matter content. Notably, under certain conditions, scalar fields, a stiff or ultra-stiff perfect fluid¹ result in generic quiescent spacelike singularities, as illustrated in the following works [1, 54, 15, 47, 18, 22] and references therein. A major reason for progress in this area is that for dimensionless variables one obtains specific temporal limits at each spatial point (i.e. temporally asymptotic spatially local self-similarity), where each spatial point evolves independently of its neighbours. However, for a broad range of other types of matter, the situation is much more complicated.

As regards generic spacelike singularities², the heuristic analysis of Belinskiĭ, Khalatnikov and Lifshitz (BKL) [39, 5, 4, 46, 60, 61] suggests the following conjectures for ‘soft’ perfect fluids (SPFs), i.e. perfect fluids with an equation of state such that the speed of sound is less than that of light:

- (i) *Vacuum domination*: Generic spacelike singularities in GR are vacuum dominated, i.e., generically SPFs asymptotically become test fields because gravity asymptotically generates more gravity than matter: ‘matter does not matter’.
- (ii) *Spatial locality*: For SPFs and vacuum models spatial points evolve independently of their neighbours asymptotically toward a generic spacelike initial singularity. More precisely, in the conformal Hubble-normalized orthonormal frame approach [55], the Hubble-normalized spatial frame derivatives asymptotically tend to zero where the limit results in the so-called local boundary, which consists of an infinite set of identical spatially homogeneous (SH) state spaces, one for each spatial point, as described in [60, 61, 43, 21].
- (iii) *Temporal oscillations*: The spatial pointwise asymptotic generic dynamics for SPFs and vacuum models are governed by oscillating sequences of Bianchi type I vacuum Kasner states mediated by Bianchi type II vacuum solutions (described by the Bianchi type I and II subsets on the local boundary), which induce a chaotic discrete *BKL* (Kasner) *map*, see e.g. [23] and references therein.³

Asymptotic spatial locality, as regards generic spacelike singularities, suggests that an understanding of SH cosmologies is essential for *inhomogeneous* cosmologies. The most general SH vacuum models are the Bianchi type VIII, IX and $VI_{-1/9}$ models, where the latter sometimes are referred to as the exceptional type VI_h models since they have an

¹A perfect fluid with a stiff (ultra-stiff) equation of state has a speed of sound that is equal to (faster than) the speed of light.

²We here focus on spacelike singularities; for null singularities see e.g. [48, 44, 11]. For the interplay between spacelike and null singularities, e.g. a singularity with both null and spacelike pieces, see e.g. [32, 6, 43, 9, 13]. For surveys on spacetime singularities and their types, see [51, 45] and references therein.

³In addition to the oscillatory local BKL behavior, we also expect joint spike oscillations, as described in [26], where the associated inhomogeneous solutions were recently found, see [41] and references therein for further details on spikes.

extra degree of freedom due to a constraint degeneracy when $h = -1/9$, see [14, Page 123, case Bbii]. In the Hubble-normalized orthonormal frame formalism, the Bianchi type VIII, IX and $VI_{-1/9}$ vacuum models possess four-dimensional state spaces and are expected to generically have initial oscillatory singularities, which is the main topic in this paper.

All Bianchi cosmologies, except Bianchi type VIII and IX, have a G_2 symmetry subgroup with two commuting spacelike Killing vector fields. This G_2 symmetry group acts orthogonally transitively in all cases, except for the general type $VI_{-1/9}$ models, which is due to their extra degree of freedom. As a consequence, the general vacuum type $VI_{-1/9}$ models are the only SH models with a SH limit of the general *inhomogeneous* vacuum models with a G_2 symmetry group.⁴ Since the general G_2 vacuum models are the simplest spatially inhomogeneous models that are expected to possess a spacelike initial singularity generically exhibiting the previous conjectures (i),(ii),(iii), addressing the general type $VI_{-1/9}$ vacuum models is arguably the most natural next step toward a deeper understanding of generic spacelike singularities.

So far, all established rigorous results concerning SH oscillatory singularities have been obtained for Bianchi type VIII and IX by using the Hubble-normalized dynamical systems approach. Ringström obtained the first proofs as regards the global asymptotics in [52, 53], see also [24]. Lately, prompted by [23], there is a series of new proofs that demonstrates the stability of various heteroclinic chains⁵ on the Bianchi type I and II boundary subsets, see [2, 37, 38, 7, 3]. Unfortunately, no analogous rigorous results are known for the general Bianchi type $VI_{-1/9}$ vacuum models, even though one expects that the Bianchi type I and II boundary subsets play a fundamental role in the asymptotic dynamics also in this case, see [30].

The type I and II boundary subsets are very different for the two classes of models, the type VIII/IX and the type $VI_{-1/9}$ models, respectively, in spite of the fact that the frame-invariant description of Kasner oscillations is described by the BKL (Kasner) map for all these vacuum models. The type VIII and IX vacuum models naturally have a (Fermi) spatial frame that is non-rotating, but this is not the case for the general type $VI_{-1/9}$ vacuum models, due to twisting and non-orthogonally transitive Killing vector fields. Hence, for the general type $VI_{-1/9}$ models the Bianchi type I and type II boundary subsets involve spatial frame rotations, which greatly complicates the heteroclinic network that these boundary subsets give rise to.

Although the general Bianchi type $VI_{-1/9}$ models have been studied before [29, 30, 28, 8], these works only involve local analysis and some numerical experiments⁶; nothing is known about the detailed structure of the heteroclinic network. In view of the recent developments [2, 37, 38, 7, 3] for Bianchi type VIII and IX, future type $VI_{-1/9}$ singularity proofs presumably rely on an analytic description of the Bianchi type I and II boundary

⁴The general G_2 models are a special case of inhomogeneous models without any symmetries when these models are expressed in an Iwasawa frame. The associated symmetry hierarchies were described in terms of invariant sets in the conformally Hubble-normalized Iwasawa frame approach given in [21]; see also [12] for the configuration space representation and description of cosmological billiards.

⁵A heteroclinic orbit is a solution trajectory that connects two different fixed points; a heteroclinic chain consists of a concatenation of heteroclinic orbits, where the ω -limit of one heteroclinic orbit is the α -limit of the next one in the chain; a heteroclinic network consists of a union of heteroclinic chains.

⁶However, rigorous results concerning quiescent singularities for stiff perfect fluids in Bianchi type $VI_{-1/9}$ were obtained in [17].

induced heteroclinic network; the primary goal of the present paper is to give such a description.

Toward this goal, we derive explicit general analytic solutions for the Bianchi type I and II subsets on the type $VI_{-1/9}$ vacuum boundary in the Hubble-normalized orthonormal frame description. We then introduce a new graphical representation in order to translate the discrete frame-invariant BKL map dynamics to the heteroclinic chain structure induced by the type I and II boundary subsets, which makes this quite complicated structure transparent. This enables us to, e.g., identify networks of entangled cyclic heteroclinic chains and show that only some of the chains are asymptotically stable and thus asymptotically relevant, which is in contrast to the corresponding ones for the vacuum type VIII and IX models. We note that there are no previous analytic descriptions of type $VI_{-1/9}$ cyclic heteroclinic chains, although some period 13 and 18 cycles were identified numerically in [8].

The paper is organized as follows. In Section 2 we describe the general Bianchi type $VI_{-1/9}$ models in the Hubble-normalized dynamical systems formalism and depict the stratification of the invariant sets. Section 3 discusses the discrete chaotic frame-invariant dynamics induced by the Bianchi type I and II boundary subsets; in addition, we show how this frame-invariant dynamics can be translated to the heteroclinic chain networks by means of a new graphical representation, which helps illustrating the heteroclinic structure in terms of state space projections. In particular, we show that only some of the chains are asymptotically stable. In Section 4 we provide some examples of networks of entangled cyclic heteroclinic chains. Appendix A contains a convenient toy model that helps obtaining the full solutions for the frame rotating Bianchi type I and II boundary subsets. In addition we derive a new monotonic function for the invariant hypersurface orthogonal subset.

2. The dynamical system and its stratification of invariant sets

To obtain the dynamical system for the Bianchi type $VI_{-1/9}$ vacuum models, we follow⁷ the conventions and the Bianchi type $VI_{-1/9}$ conditions in [21, 26]. We hence write $\Sigma_\alpha = \Sigma_{\alpha\alpha}$, $\alpha = 1, 2, 3$, and use a *time variable* τ directed toward the past singularity.⁸ However, to simplify the Gauss constraint, given below, we perform the following rescaling $A_3 \mapsto A/2$, $R_1 \mapsto \sqrt{3}R_1$ and $R_3 \mapsto \sqrt{3}R_3$ of the variables in [21, 26] and set $N_- := N_1/2\sqrt{3} = N_{11}/2\sqrt{3}$; the equations for the Bianchi type $VI_{-1/9}$ vacuum models are then obtained by setting $N_{12} = 3A/2$ and $R_2 = 0$ in the relevant equations in [21, 26], which yields the

⁷As in [21, 26] we use the Iwasawa frame $\mathbf{e}_1 = e_1^1\partial_x$, $\mathbf{e}_2 = e_2^1\partial_x + e_2^2\partial_y$, $\mathbf{e}_3 = e_3^1\partial_x + e_3^2\partial_y + e_3^3\partial_z$ while Hewitt, Horwood, Wainwright (HHW) [30] used $\mathbf{e}_1 = e_1^1\partial_x + e_1^2\partial_y + e_1^3\partial_z$, $\mathbf{e}_2 = e_2^2\partial_y$, $\mathbf{e}_3 = e_3^2\partial_y + e_3^3\partial_z$ as the spatial frame, which corresponds to a permutation of the spatial axes. Instead of using the systems in [21, 26], the system (1), (2) can be obtained from eqs. (2.8), (2.10), (2.2) in HHW by noticing the following relationship between the present variables and those in HHW: $(\Sigma_1, \Sigma_2, \Sigma_3, R_1, R_3, N_-, A) = (\Sigma_+ + \sqrt{3}\Sigma_-, \Sigma_+ - \sqrt{3}\Sigma_-, -2\Sigma_+, -\Sigma_2, -\Sigma_\times, N_-, 2A)_{HHW}$.

⁸Hence $\tau = -N$, where N represents the forward directed e -fold time variable used in [30] where N was called τ , which hence is the negative of the present τ .

following *evolution equations*:

$$\begin{aligned}
(1a) \quad & \Sigma'_1 = 2(1 - \Sigma^2)\Sigma_1 - 6R_3^2 + 8N_-^2, \\
(1b) \quad & \Sigma'_2 = 2(1 - \Sigma^2)\Sigma_2 + 6R_3^2 - 6R_1^2 - 4N_-^2 + 3A^2, \\
(1c) \quad & \Sigma'_3 = 2(1 - \Sigma^2)\Sigma_3 + 6R_1^2 - 4N_-^2 - 3A^2, \\
(1d) \quad & R'_1 = [2(1 - \Sigma^2) + \Sigma_2 - \Sigma_3]R_1, \\
(1e) \quad & R'_3 = [2(1 - \Sigma^2) + \Sigma_1 - \Sigma_2]R_3 - 4N_-A, \\
(1f) \quad & N'_- = -2(\Sigma^2 + \Sigma_1)N_- + 3R_3A, \\
(1g) \quad & A' = -(2\Sigma^2 - \Sigma_3)A,
\end{aligned}$$

where the state vector $(\Sigma, \Sigma_1, \Sigma_2, \Sigma_3, R_1, R_3, N_-, A) \in \mathbb{R}^7$ is subject to the following *constraint equations*

$$\begin{aligned}
(2a) \quad & 1 - \Sigma^2 - N_-^2 - A^2 = 0, \\
(2b) \quad & 2R_3N_- + \Sigma_1A = 0, \\
(2c) \quad & \Sigma_1 + \Sigma_2 + \Sigma_3 = 0,
\end{aligned}$$

where

$$(3) \quad \Sigma^2 := \frac{1}{6} (\Sigma_1^2 + \Sigma_2^2 + \Sigma_3^2) + R_1^2 + R_3^2.$$

Due to the constraints (2), all variables are bounded and the state space is 4-dimensional. As shown in [30], discrete symmetries allow us to, without loss of generality, assume that

$$(4) \quad R_1 \geq 0, \quad A \geq 0,$$

but note that since Σ_1 can change sign so can R_3N_- and hence $R_3N_- = 0$ is not, in general, an invariant set when $A > 0$. This, however, leads to multiple equivalent representations of some of the invariant subsets on the state space boundary. Finally, we note that the *deceleration parameter* q is given by

$$(5) \quad q = 2\Sigma^2.$$

The constrained dynamical system (1), (2) admits several *explicitly known invariant sets* of various dimensions (see Figure 1):

- (a) The Bianchi type I *Kasner* boundary subset, for which $A = N_- = 0$, denoted by $\mathcal{B}_I = \mathcal{K}$. In this case, the constraint (2b) is trivially satisfied. This set consists of the union of the following subsets:
 - (i) The 1D Kasner circle of fixed points, K° , where $R_1 = R_3 = 0$.
 - (ii) The 2D single frame transition subsets, denoted by \mathcal{T}_{R_1} and \mathcal{T}_{R_3} , which respectively occur when $R_1 > 0, R_3 = 0$; $R_1 = 0, R_3 > 0$ and $R_1 = 0, R_3 < 0$, where \mathcal{T}_{R_3} consists of two disjoint components related by the symmetry $R_3 \mapsto -R_3$.
 - (iii) The 3D double frame transition subset, denoted by $\mathcal{T}_{R_1R_3}$, consisting of two disjoint components, $R_1R_3 > 0$ and $R_1R_3 < 0$, related by the symmetry $R_3 \mapsto -R_3$.
- (b) The Bianchi type II boundary subset, characterized by $R_3 = A = 0$ and designated by \mathcal{B}_{II} . Again, the constraint (2b) is trivially satisfied. This set is the union of the following subsets:

- (i) The 2D single curvature transition subset, denoted by \mathcal{T}_{N_-} , which occurs when $R_1 = 0$, with two disjoint components, $N_- > 0$ and $N_- < 0$, related by the symmetry $N_- \mapsto -N_-$.
- (ii) The 3D mixed curvature-frame transition subset, denoted by $\mathcal{T}_{R_1 N_-}$, consisting of two disjoint components, $R_1 N_- > 0$ and $R_1 N_- < 0$, related by the symmetry $N_- \mapsto -N_-$.
- (c) The 3D *orthogonally transitive* subset \mathcal{OT} , which is defined by $R_1 = 0$. In particular, it contains the 1D arc of type VI $_{-1/9}$ plane wave fixed points PW^\pm .
- (d) The 2D *hypersurface orthogonal* subset, \mathcal{HO} , characterized by $n^\alpha_\alpha = 0$ and hence $N^\alpha_\alpha = 0$, see e.g. [63]. This subset corresponds to that one of the Killing vector fields of the Abelian G_2 subgroup of symmetries is hypersurface orthogonal. In the present variables, the \mathcal{HO} subset is given by $\Sigma_1 = R_3 = N_- = 0$. This subset admits the 1D *shear diagonal and Fermi-propagated* subset, \mathcal{D} , in which both of the two Killing vector fields forming the Abelian G_2 symmetry group are hypersurface orthogonal, which follows from the intersection of the \mathcal{HO} and \mathcal{OT} subsets. In the present variables, \mathcal{D} is described by $\Sigma_1 = R_1 = R_3 = N_- = 0$. The \mathcal{HO} subset also contains the Robinson-Trautman fixed point, denoted by RT.

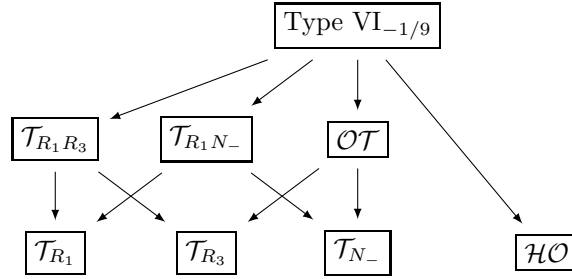


Figure 1: The invariant set stratification of the general Bianchi type VI $_{-1/9}$ vacuum models. From the general 4D models to the 3D and 2D subsets obtained by setting certain variables to zero. Subsequent intersections of the closure of these subsets yield lower dimensional subsets, e.g. intersections of two of the $\overline{\mathcal{T}}_{R_1}$, $\overline{\mathcal{T}}_{R_3}$, $\overline{\mathcal{T}}_{N_-}$ subsets yield the 1D Kasner circle K° of fixed points, while the intersection of the \mathcal{OT} and \mathcal{HO} subsets yields the 1D subset \mathcal{D} .

Next we turn to a more detailed description of the above invariant subsets. First, we describe the fixed points and their stability.

2.1. Sets of fixed points

The system (1), (2) admits several sets of fixed points:

RT The Robinson-Trautman Bianchi type VI $_{-1/9}$ fixed point:⁹

$$(6) \quad \text{RT} := \left\{ (\Sigma_1, \Sigma_2, \Sigma_3, R_1, R_3, N_-, A) = \left(0, -\frac{2}{3}, \frac{2}{3}, \frac{\sqrt{5}}{3\sqrt{3}}, 0, 0, \sqrt{\frac{2}{3}} \right) \right\}.$$

⁹The Robinson-Trautman solution, belonging to Petrov type III, is also associated with the name Collinson-French, see [29, 28]; for a discussion about its properties see [59, Ch. 28, p. 200].

This fixed point resides in the \mathcal{HO} subset. The deceleration parameter takes the value $q = 2/3$, according to (5). Linear analysis shows that this fixed point is a local source (with respect to the present past time direction τ).

PW $^\pm$ The arc of type VI $_{-1/9}$ plane wave fixed points is parametrized by a constant value of $\Sigma_1 \in (-1, 0]$ and is given by

$$(7) \quad \text{PW}^\pm := \left\{ \begin{array}{l} (\Sigma_2, \Sigma_3, A) = \frac{1}{2}(-3 + \Sigma_1, 3 - \Sigma_1, 1 + \Sigma_1), \\ (R_1, R_3, N_-) = \pm \frac{1}{2} \sqrt{-\Sigma_1(\Sigma_1 + 1)} (0, 1, 1) \end{array} \mid \Sigma_1 \in (-1, 0] \right\},$$

where $q = (3 - \Sigma_1)/2$. The fixed points PW $^\pm$ belong to the invariant orthogonally transitive subset, \mathcal{OT} , with $R_1 = 0$. The special PW $^\pm$ fixed point with $\Sigma_1 = 0$, given by

$$(8) \quad \text{PW}^0 := \left\{ (\Sigma_1, \Sigma_2, \Sigma_3, R_1, R_3, N_-, A) = \frac{1}{2}(0, -3, 3, 0, 0, 0, 1) \right\},$$

divides the arc PW $^\pm$ into two equivalent branches, PW $^+$ and PW $^-$; one with positive values and one with negative values of R_3 and N_- , related by the symmetry $(R_3, N_-) \mapsto -(R_3, N_-)$. Note that PW 0 resides in the 1D invariant shear diagonalized Fermi-propagated subset \mathcal{D} , which corresponds to an intersection of the \mathcal{OT} and \mathcal{HO} subsets. The limit $\Sigma_1 \rightarrow -1$ corresponds to that PW $^+$ and PW $^-$ approach the Taub point T_3 discussed below, which thereby leads to a closed arc of fixed points.

A linear analysis reveals that the fixed points PW $^\pm$ is a center-source (with respect to τ) on the \mathcal{OT} subset with $R_1 = 0$, whereas R_1 yields a stable direction, as seen from the linearization of the equation for R_1 at PW $^\pm$:

$$(9) \quad R_1' = -\frac{1}{2}(5 - \Sigma_1) R_1,$$

since $-\frac{1}{2}(5 - \Sigma_1) \in (-3, -\frac{5}{2}]$.

K $^\circ$ Setting $R_1 = R_3 = N_- = A = 0$ yields the circle of Kasner fixed points,

$$(10) \quad \text{K}^\circ := \left\{ (\Sigma_1, \Sigma_2, \Sigma_3, 0, 0, 0, 0) \in \mathbb{R}^7 \mid \begin{array}{l} 1 - \Sigma^2 = 0, \\ \Sigma_1 + \Sigma_2 + \Sigma_3 = 0 \end{array} \right\}.$$

The Kasner circle is conveniently parametrized by the Kasner parameters p_α with $\alpha = 1, 2, 3$, which are defined by $\Sigma_\alpha = 3p_\alpha - 1$, satisfying the Kasner relations

$$(11) \quad p_1 + p_2 + p_3 = 1, \quad p_1^2 + p_2^2 + p_3^2 = 1.$$

It follows that the deceleration parameter in (5) is given by $q = 2$.

The Kasner circle K $^\circ$ is naturally divided into six equivalent sectors, associated with axes permutations, denoted by permutations of the triple (123) where each sector $(\alpha\beta\gamma)$ is defined by¹⁰

$$(12) \quad -\frac{1}{3} < p_\alpha < 0 < p_\beta < \frac{2}{3} < p_\gamma < 1,$$

¹⁰Note that our spatial frame choice is related to the one of HHW in [30] by a permutation of the spatial axes such that the present convention with (123) yields (231) in [30], i.e., $(123) \leftrightarrow (231)_{\text{HHW}}$.

see Figure 2. The boundaries of the sectors are six special points that are associated with locally rotationally symmetric (LRS) solutions (they are even plane symmetric solutions, since the spatial curvature is flat for Bianchi type I),

$$(13a) \quad \boxed{T_\alpha} \quad (\Sigma_\alpha, \Sigma_\beta, \Sigma_\gamma) = (2, -1, -1), \quad \text{or} \quad (p_\alpha, p_\beta, p_\gamma) = (1, 0, 0);$$

$$(13b) \quad \boxed{Q_\alpha} \quad (\Sigma_\alpha, \Sigma_\beta, \Sigma_\gamma) = (-2, 1, 1), \quad \text{or} \quad (p_\alpha, p_\beta, p_\gamma) = \left(-\frac{1}{3}, \frac{2}{3}, \frac{2}{3}\right).$$

The *Taub points* T_α , $\alpha = 1, 2, 3$, correspond to the flat LRS solutions — the Taub representation of the Minkowski spacetime, while Q_α , $\alpha = 1, 2, 3$, yield three equivalent LRS solutions with non-flat geometry.

It is convenient to parametrize the Kasner parameters p_1, p_2, p_3 by the *frame-invariant Kasner parameter* u , which is frame-invariantly defined by the relation¹¹

$$(14) \quad \det(\Sigma_{\alpha\beta}) = 2 + 27p_1p_2p_3 = 2 - \frac{27u^2(1+u)^2}{f^3(u)}, \quad u \in [1, \infty],$$

where the function $f(x)$ is defined as

$$(15) \quad f(x) := 1 + x + x^2,$$

and hence $\det(\Sigma_{\alpha\beta})$ is a monotonically increasing function in u . Due to frame invariance, the Kasner parameter u naturally captures the equivalence of the six sectors of K° . On sector $(\alpha\beta\gamma)$, where $p_\alpha < p_\beta < p_\gamma$, we set

$$(16) \quad p_\alpha = -\frac{u}{f(u)}, \quad p_\beta = \frac{1+u}{f(u)}, \quad p_\gamma = \frac{u(1+u)}{f(u)},$$

where $u \in (1, \infty)$. The boundary points of sector $(\alpha\beta\gamma)$, Q_α and T_γ , are characterized by $u = 1$ and $u = \infty$, respectively.

Note that the magnetic Weyl tensor is identically zero on the Kasner subset, but the electric part is non-trivial and leads a non-zero quadratic Weyl (Kretschmann, since we consider vacuum) scalar that is related to $\det(\Sigma_{\alpha\beta})$ according to

$$(17) \quad \mathcal{W} := \frac{C_{abcd}C^{abcd}}{48H^4} = 2 - \det(\Sigma_{\alpha\beta}) = \frac{27u^2(1+u)^2}{f^3(u)} = \text{const.},$$

which thereby also yields a frame-invariant description of the various Kasner states. For large u , and thereby small \mathcal{W} , it follows that $\mathcal{W} = 27u^{-1}(1 + u^{-1} + O(u^{-2}))$.

In addition to the standard Kasner parameter u , which parametrize each sector $(\alpha\beta\gamma)$ as in (16), it is useful to define the *extended Kasner parameter* \check{u} , which parametrizes the whole Kasner circle, by setting

$$(18) \quad p_1 = -\frac{\check{u}}{f(\check{u})}, \quad p_2 = \frac{1+\check{u}}{f(\check{u})}, \quad p_3 = \frac{\check{u}(1+\check{u})}{f(\check{u})},$$

where $\check{u} \in (-\infty, \infty)$, so that each value of \check{u} distinguishes a unique point on the Kasner circle K° . Comparing (16) and (18) we obtain a transformation between u and \check{u} for each sector:

¹¹For the BKL definition of u , the order of p_α is fixed according to $p_1 \leq p_2 \leq p_3$; we find it convenient to use the above frame independent definition instead, and to permute the ordering of p_α according to the sector one considers when dealing with frame-dependent matters.

Sector	Parameter \check{u}	Range of \check{u}	$u = 2$
(213)	$\check{u} = -(1 + u)$	$\check{u} \in (-\infty, -2)$	$\check{u} = -3$
(231)	$\check{u} = -\frac{1+u}{u}$	$\check{u} \in (-2, -1)$	$\check{u} = -\frac{3}{2}$
(321)	$\check{u} = -\frac{u}{1+u}$	$\check{u} \in (-1, -\frac{1}{2})$	$\check{u} = -\frac{2}{3}$
(312)	$\check{u} = -\frac{1}{1+u}$	$\check{u} \in (-\frac{1}{2}, 0)$	$\check{u} = -\frac{1}{3}$
(132)	$\check{u} = \frac{1}{u}$	$\check{u} \in (0, 1)$	$\check{u} = \frac{1}{2}$
(123)	$\check{u} = u$	$\check{u} \in (1, \infty)$	$\check{u} = 2$

Correspondence	
\check{u}	Point
$-\infty$	T_3
-2	Q_2
-1	T_1
$-1/2$	Q_3
0	T_2
1	Q_1
∞	T_3

Table 1: Parametrization of each sector $(\alpha\beta\gamma)$ of the Kasner circle K° by the extended Kasner parameter \check{u} , and the values of \check{u} for the different LRS points on K° , which constitute the boundaries of the different sectors $(\alpha\beta\gamma)$. We also describe the six representations of $u = 2$, one in each sector, where $u = 2$ yields the boundary of $1 < u < 2$, which signifies the last Kasner state in a frame-invariant Kasner era, discussed below.

Note that even though the different sectors $(\alpha\beta\gamma)$ yield equivalent solutions, due to the permutation symmetries inherited from permutations of the spatial axes, we will see that they play different roles for the global past dynamics of the present dynamical system (1), (2). We pursue the stability of K° next.

Linearization of the system (1) at an arbitrary point $(p_1, p_2, p_3) \in K^\circ$ yields

$$(19a) \quad R'_1 = 3(p_2 - p_3)R_1 = \lambda_{R_1}R_1, \quad \lambda_{R_1} := \frac{3(1 - \check{u}^2)}{f(\check{u})},$$

$$(19b) \quad R'_3 = 3(p_1 - p_2)R_3 = \lambda_{R_3}R_3, \quad \lambda_{R_3} := -\frac{3(1 + 2\check{u})}{f(\check{u})},$$

$$(19c) \quad N'_- = -6p_1N_- = \lambda_{N_-}N_-, \quad \lambda_{N_-} := \frac{6\check{u}}{f(\check{u})},$$

$$(19d) \quad A' = -3(1 - p_3)A = \lambda_A A, \quad \lambda_A := -\frac{3}{f(\check{u})}.$$

The analysis of the stability of the Kasner circle K° is summarized in Figure 2, where the unstable variables in τ are given for each sector of K° . Note that each of the variables R_1, R_3, N_- trigger instability in different parts of the Kasner circle, although there is some overlap between these parts, which is similar to the subcritical case of the Bianchi type VIII and IX Hořava-Lifshitz models discussed in [27, 36, 10]. On the other hand, the variable A does not trigger any instability nearby the Kasner circle, since its corresponding eigenvalue $\lambda_A < 0$ for all $\check{u} \in \mathbb{R}$, while $\lambda_A = 0$ at T_3 where $\check{u} = \pm\infty$. Since R_3, N_- and A yield center-eigendirections at the Taub point T_3 , it follows that understanding the dynamics in the vicinity of T_3 poses challenges. Note that the above remarks did not take into account the Codazzi constraint (2b).¹²

¹²On the one hand, linearization of (2b) at K° yields $(3p_1 - 1)A = 0$, since $N_-R_3 = 0$ at linear order. This results in that A is zero to linear order except at $p_1 = \frac{1}{3}$ (i.e. at $\Sigma_1 = 0$), which amounts to the Kasner fixed points K°_\pm on the shear diagonal and Fermi-propagated subset \mathcal{D} . On the other hand, introducing N_-R_3 as an auxiliary variable and linearizing at K° yields $(N_-R_3)' = -3(1 - p_3)(N_-R_3) = \lambda_A(N_-R_3)$, which explains why $\lambda_A = \lambda_{N_-} + \lambda_{R_3}$.

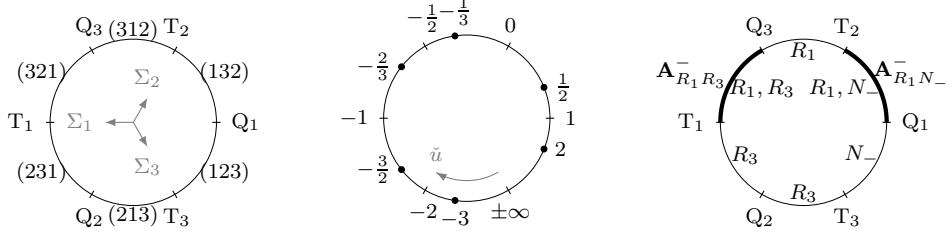


Figure 2: **Left:** Description of the Kasner circle K° sectors $(\alpha\beta\gamma)$, where a sector $(\alpha\beta\gamma)$ has a boundary consisting of the points Q_α and T_γ , where $\alpha\beta\gamma$ is a permutation of 123. **Middle:** We describe Q_α , T_γ and the six representations of $u = 2$ in terms of the extended Kasner parameter \tilde{u} . The parameter \tilde{u} starts at T_3 with value $\tilde{u} = -\infty$ and increases with a clock-wise rotation until it reaches T_3 again when $\tilde{u} = +\infty$, see Table 1. **Right:** Inside K° , we describe the variables that trigger instability in each sector: In the (thin) sectors, there is a single unstable variable while the (bold) sectors, denoted by $\mathbf{A}_{R_1 N_-}^- := (132)$ and $\mathbf{A}_{R_1 R_3}^- := (321)$, exhibit two unstable variables.

2.2. The Kasner subset \mathcal{K}

The shear diagonalized Fermi-propagated representation of the Kasner solutions on the Kasner circle K° of the Kasner boundary subset, \mathcal{K} , is not the only one. With respect to the present Iwasawa frame with $R_2 = 0$, they can also be expressed in a rotating spatial frame, which then leads to time dependent non-diagonal Hubble-normalized shear with non-zero R_1 or/and non-zero R_3 , but with $N_- = A = 0$. However, the shear frame-invariants, i.e., the trace, the trace of its square, and the determinant of the shear, are constant, since they can also be expressed in the shear diagonalized Fermi-propagated frame and thereby subsequently by the frame-invariant parameter u . It hence follows from (2) and (14) that the Kasner solutions obey the relations:

$$(20a) \quad 0 = \Sigma_1 + \Sigma_2 + \Sigma_3,$$

$$(20b) \quad 1 = \frac{1}{6} (\Sigma_1^2 + \Sigma_2^2 + \Sigma_3^2) + R_1^2 + R_3^2,$$

$$(20c) \quad \det \Sigma_{\alpha\beta} = \Sigma_1 \Sigma_2 \Sigma_3 - 3\Sigma_1 R_1^2 - 3\Sigma_3 R_3^2 = 2 - \frac{27u^2(1+u)^2}{f^3(u)},$$

where we recall that $u \in [1, \infty]$.¹³

We refer to heteroclinic orbits in \mathcal{K} that connect two different fixed points on K° with either $R_1 \neq 0$, $R_3 = 0$ or $R_1 = 0$, $R_3 \neq 0$ as *single frame transitions*. These individual orbits and collectively as 2D invariant subsets, are denoted by \mathcal{T}_{R_1} and \mathcal{T}_{R_3} , respectively. We now describe the dynamics of these subsets.

The single frame transitions ‘triggered’ by the instability of $R_1 > 0$ yield a frame rotation in the (2–3)-plane. This results in that $\Sigma_1 = 3p_1 - 1 = -(1 + 4\tilde{u} + \tilde{u}^2)/f(\tilde{u}) = \text{constant}$ is invariant, where $\tilde{u} = \tilde{u}_- \in (-1, 1)$ denotes the fixed point on K° from where a particular heteroclinic orbit \mathcal{T}_{R_1} originates, as follows from (1a) and (20c), where the latter can be rewritten as $\det \Sigma_{\alpha\beta} = \Sigma_1(\Sigma_1^2 - 3) + 3(\Sigma_1 - \Sigma_3)R_3^2$, in which setting $R_3 = 0$ yields $\Sigma_1 = \text{constant}$. Such an orbit is represented by a single straight line in $(\Sigma_1, \Sigma_2, \Sigma_3)$ -space with Σ_3 (resp. Σ_2) monotonically increasing (resp. decreasing) in τ , resulting in a total

¹³Using the variables of Hewitt et al. given in footnote 7 and solving for $R_3^2 = \Sigma_x^2$ in eq. (20b) and inserting the result into (20c) leads to an expression that is equivalent to eq. (5.5) in [30].

frame rotation with $\pi/2$ in the $(2-3)$ -plane, thereby permuting the indices 2 and 3. The frame transitions \mathcal{T}_{R_1} thereby originate from the Kasner arc $\mathbf{A}_{R_1}^-$, on which R_1 is unstable on K° , which is parametrized by $\check{u}_- \in (-1, 1)$ and consisting of the sectors (132), (312), (321) and the fixed points Q_3, T_2 , whereas they end at the Kasner arc $\mathbf{A}_{R_1}^+$, which is parametrized by \check{u}_+ such that $|\check{u}_+| > 1$, obtained by interchanging 2 and 3 in the description of $\mathbf{A}_{R_1}^-$, see Figure 3.

Analogous statements hold for the \mathcal{T}_{R_3} transitions in either of the two equivalent disjoint subsets, $R_3 > 0$ and $R_3 < 0$. Thus frame rotations in the $(1-2)$ -plane result in straight lines in $(\Sigma_1, \Sigma_2, \Sigma_3)$ -space such that $\Sigma_3 = 3p_3 - 1 = -(1 - 2\check{u} - 2\check{u}^2)/f(\check{u}) = \text{constant}$, $\check{u} = \check{u}_- \in (-\infty, -1/2)$ where Σ_2 (resp. Σ_1) is monotonically increasing (resp. decreasing) in τ . These frame transitions hence originate from the Kasner arc $\mathbf{A}_{R_3}^-$, consisting of the sectors (213), (231), (321) and the fixed points Q_2, T_1 , and end at the Kasner arc $\mathbf{A}_{R_3}^+$ parametrized by $\check{u} = \check{u}_+ \in (-1/2, +\infty)$, obtained from $\mathbf{A}_{R_3}^-$ by interchanging 1 and 2, see Figure 3. Finally, note that the \mathcal{T}_{R_3} transitions become tangential to the Kasner circle K° at T_3 , which is the reason for the zero eigenvalue at T_3 associated with R_3 , see Figure 3.

Heteroclinic orbits with $R_1 R_3 > 0$ or $R_1 R_3 < 0$ are called *double frame transitions*. These individual orbits and collectively as two equivalent invariant 3D subsets, are denoted by $\mathcal{T}_{R_1 R_3}$. The variable Σ_3 (resp. Σ_1) is monotonically increasing (resp. decreasing) for these transitions, which together with the linear analysis of K° establishes that this 2-parameter set of orbits is described by two equivalent 1-parameter sets of orbits (one with $R_3 < 0$ and one with $R_3 > 0$) that originates from each of the fixed points on the Kasner arc $\mathbf{A}_{R_1 R_3}^-$, given by sector (321) and parametrized by $\check{u}_- \in (-1, -1/2)$, while they end at the arc $\mathbf{A}_{R_1 R_3}^+$, given by sector (123) described by $\check{u}_+ \in (1, +\infty)$. Note that the invariant $\mathcal{T}_{R_1 R_3}$ set is bounded by the single frame transition \mathcal{T}_{R_1} and \mathcal{T}_{R_3} Kasner subsets. The final result is obtained by interchanging Σ_1 and Σ_3 .

These results can be summarized as follows:

Lemma 2.1. *All \mathcal{T}_{R_1} (resp. \mathcal{T}_{R_3} and $\mathcal{T}_{R_1 R_3}$) orbits possess an α -limit set that resides in the subset $\mathbf{A}_{R_1}^- \subseteq K^\circ$ (resp. $\mathbf{A}_{R_3}^- \subseteq K^\circ$ and $\mathbf{A}_{R_1 R_3}^- \subseteq K^\circ$) of the Kasner circle K° , whereas its ω -limit set resides in $\mathbf{A}_{R_1}^+ \subseteq K^\circ$ (resp. $\mathbf{A}_{R_3}^+ \subseteq K^\circ$ and $\mathbf{A}_{R_1 R_3}^+ \subseteq K^\circ$).*

Finally, as shown in Appendix A.2, there exists a discrete symmetry, which corresponds to interchanging the indices 1 and 3 together with $(\Sigma_1, \Sigma_2, \Sigma_3) = -(\Sigma_1, \Sigma_2, \Sigma_3)$, or letting $\tau \rightarrow -\tau$. Moreover, there exists a special orbit, for which $R_1 = R_3, \Sigma_2 = 0, \Sigma_3 = -\Sigma_1$, that originates from $\Sigma_1 = \sqrt{3}$ and ends at $\Sigma_1 = -\sqrt{3}$ (where, as for all double frame transitions, Σ_1 is monotonically decreasing), which correspond to $\check{u}_- = 1 - \sqrt{3}$ and $\check{u}_+ = 1 + \sqrt{3}$, respectively, where \check{u}_+ and \check{u}_- correspond to $u = 1 + \sqrt{3}$, since \check{u}_+ is in sector (123). The projection of this orbit in $(\Sigma_1, \Sigma_2, \Sigma_3)$ -space is a straight line, see Figure 3 (right). Although the double frame transitions $\mathcal{T}_{R_1 R_3}$ satisfy (20), one more constant of the motion is needed to describe them completely. It is possible to obtain all of the double frame transition orbits explicitly by means of a coordinate transformation of the Kasner solutions in a shear diagonalized Fermi-propagated frame with $R_1 = R_3 = 0$, as shown by Lim [40], see also [42]. We present the solutions in a simple explicit form in the present variables in Appendix A.2.

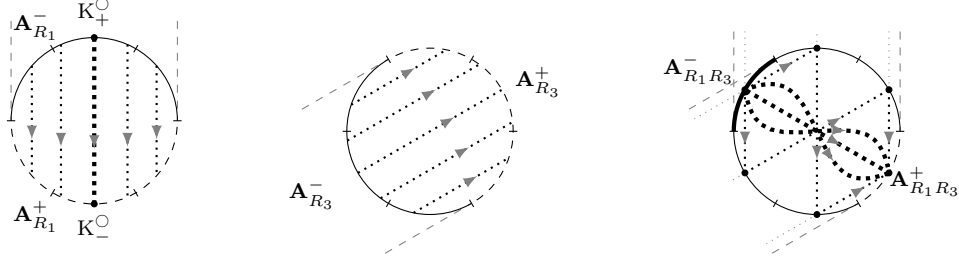


Figure 3: Projection of heteroclinic frame transition orbits onto the plane $\Sigma_1 + \Sigma_2 + \Sigma_3 = 0$ in $(\Sigma_1, \Sigma_2, \Sigma_3)$ -space. **Left and Middle:** The single frame transitions occur when either $R_1 > 0$ (left) or $R_3 \neq 0$ (middle). The α -limit set when $R_1 > 0$ (resp. $R_3 \neq 0$) is a fixed point in the arc $\mathbf{A}_{R_1}^-$ (resp. $\mathbf{A}_{R_3}^-$), whereas the ω -limit set is a fixed point in the (dashed) stable set denoted by $\mathbf{A}_{R_1}^+$ (resp. $\mathbf{A}_{R_3}^+$). The special heteroclinic \mathcal{T}_{R_1} orbit $K_+^0 \rightarrow K_-^0$, which occurs when $\Sigma_1 = 0$, plays a special role, since it forms one of the boundaries of the \mathcal{HO} subset, see Figure 6. **Right:** A double frame transition, which occurs when $R_1 R_3 > 0$ or $R_1 R_3 < 0$ (right), yields two equivalent 1-parameter sets of orbits with an α -limit set given by a fixed point in the arc $\mathbf{A}_{R_1 R_3}^- := (321)$, whereas the ω -limit of these orbits is a fixed point in the stable Kasner set denoted by $\mathbf{A}_{R_1 R_3}^+ := (123)$.

2.3. The Bianchi type II subset \mathcal{B}_{II}

The Bianchi type II subset \mathcal{B}_{II} is obtained by setting $A = 0 = R_3$. Fermi-propagated solutions ($R_1 = R_2 = R_3 = 0$) such that $N_- > 0$ or $N_- < 0$ yield heteroclinic orbits triggered by the instability of the variable N_- . We refer to these individual orbits and collectively as an invariant subset with two disjoint components, as *single curvature transitions* that are denoted by \mathcal{T}_{N_-} . These heteroclinic orbits originate from the Kasner arc $\mathbf{A}_{N_-}^-$ parametrized by $\check{u}_- \in (0, +\infty)$, which consists of the sectors (123), (132) and the fixed point Q_1 , and then end at the Kasner arc $\mathbf{A}_{N_-}^+$, which is the open complement of the $\mathbf{A}_{N_-}^-$ arc on K^0 parametrized by $\check{u}_+ \in (-\infty, 0)$. They are straight lines in $(\Sigma_1, \Sigma_2, \Sigma_3)$ -space, see Figure 4, conveniently parametrized as follows (see [21]):

$$(21) \quad \Sigma_1 = -4 + (1 + \check{u}_-^2)\zeta, \quad \Sigma_2 = 2 - \check{u}_-^2\zeta, \quad \Sigma_3 = 2 - \zeta,$$

where $\check{u}_- \in (0, +\infty)$ parametrizes the initial Kasner states, and the parameter ζ evolves according to

$$(22) \quad \zeta' = 2(1 - \Sigma^2) = 6 \left(1 - \frac{\zeta}{\zeta_+}\right) \left(\frac{\zeta}{\zeta_-} - 1\right),$$

where $\zeta_{\pm} := 3/f(\mp\check{u})$. Thus, ζ is monotonically increasing from ζ_- to ζ_+ . The variable N_- is determined by the constraint

$$(23) \quad \frac{1}{6} (\Sigma_1^2 + \Sigma_2^2 + \Sigma_3^2) + N_-^2 = 1.$$

Finally note that the single curvature transitions \mathcal{T}_{N_-} become tangential to T_3 , which explains the zero eigenvalue associated with N_- at T_3 .

The Bianchi type II vacuum models assume a less transparent form in an Iwasawa frame that is rotating with respect to a Fermi-propagated frame with $R_1 > 0$. In this case the solutions are called *mixed curvature-frame transitions*, denoted by $\mathcal{T}_{R_1 N_-}$, since $N_- \neq 0$ and $R_1 \neq 0$ simultaneously. Combining the linearization results of K^0 with the fact that Σ_1 is

monotonically increasing¹⁴ leads to the conclusion that mixed curvature-frame transitions originate from the Kasner arc $\mathbf{A}_{R_1 N_-}^-$, which is the Kasner sector (132) parametrized by $\check{u}_- \in (0, 1)$, and end at the Kasner arc $\mathbf{A}_{R_1 N_-}^+$, given by the Kasner sectors (213), (231) and Q_2 , which is parametrized by $\check{u}_+ \in (-\infty, -1)$. Since the boundary of the Bianchi type II set with $R_1 N_- \neq 0$ is given by the union of the subsets $R_1 = 0$ and $N_- = 0$, the final state on K° of a $\mathcal{T}_{R_1 N_-}$ transition coincides with the Kasner circle point obtained by successively applying the single curvature and frame transitions of the boundary of $\mathcal{T}_{R_1 N_-}$. As in the case of double frame transitions, single transitions act as building blocks that determine the final result of multiple transitions, see Figure 4. These results can be summarized as follows:

Lemma 2.2. *All \mathcal{T}_{N_-} (resp. $\mathcal{T}_{R_1 N_-}$) orbits possess an α -limit set that lies in $\mathbf{A}_{N_-}^- \subseteq K^\circ$ (resp. $\mathbf{A}_{R_1 N_-}^- \subseteq K^\circ$), whereas its ω -limit set resides in $\mathbf{A}_{N_-}^+ \subseteq K^\circ$ (resp. $\mathbf{A}_{R_1 N_-}^+ \subseteq K^\circ$).*

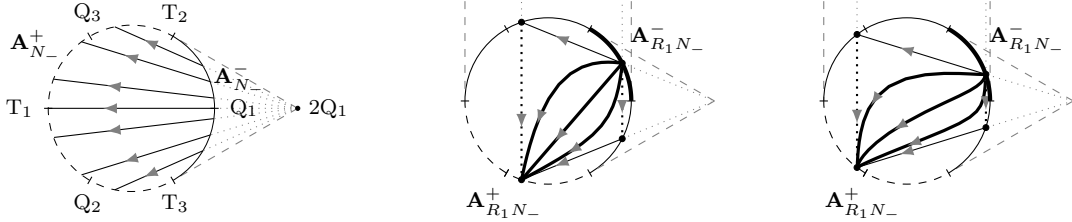


Figure 4: Projection of Bianchi type II heteroclinic orbits onto the plane $\Sigma_1 + \Sigma_2 + \Sigma_3 = 0$ in $(\Sigma_1, \Sigma_2, \Sigma_3)$ -space. **Left:** the single curvature transitions occur when $N_- \neq 0$: the α -limit set is a fixed point in the arc $\mathbf{A}_{N_-}^- := (132) \cup (123) \cup Q_2$, whereas the ω -limit set is a fixed point in the (dashed) stable set denoted by $\mathbf{A}_{N_-}^+$. **Middle:** the mixed curvature-frame transitions occur when $R_1 N_- \neq 0$. A mixed curvature-frame transition yields two equivalent 1-parameter set of orbits, related by $N_- \mapsto -N_-$, for which the α -limit set is a fixed point in the arc $\mathbf{A}_{R_1 N_-}^- := (132)$, whereas the ω -limit set is a fixed point in the (dashed) stable set denoted by $\mathbf{A}_{R_1 N_-}^+ := (231) \cup (213) \cup Q_2$. We display the case of mixed curvature-frame transitions with the α -limit given by the Kasner fixed point with $\check{u} = \sqrt{2} - 1$, which admit a special mixed curvature-frame transition orbit that is a straight line when projected onto the plane $\Sigma_1 + \Sigma_2 + \Sigma_3 = 0$ in $(\Sigma_1, \Sigma_2, \Sigma_3)$ -space. **Right:** another example of mixed curvature-frame transitions, where the ω -limit set is contained in sector (231) instead of sector (213), as in the middle Figure.

In Appendix A.3 we derive the general solution for this subset, as well as the following integral,

$$(24) \quad \frac{(1 + \Sigma_1)^2 + 3N_-^2}{(4 + \Sigma_1)^2} = \left(\frac{\check{u}}{1 + \check{u}^2} \right)^2,$$

where $\check{u} = \check{u}_-$ is the initial Kasner state of the transition and where this expression also holds for the single curvature transitions \mathcal{T}_{N_-} for which $\check{u} = \check{u}_- \in (0, +\infty)$.¹⁵

We note that at $\check{u} = \sqrt{2} - 1 \in (132)$, there are two equal unstable eigenvalues $\lambda_{R_1} = \lambda_{N_-}$. At this value of \check{u} , as for all values of $\check{u} \in (132)$, there are two equivalent 1-parameter

¹⁴Note that the equation for Σ_1 is the same for single curvature and mixed curvature-frame transitions, due to that Σ_1 is unaffected by rotations induced by R_1 in the $(2 - 3)$ -plane. For additional details, see Appendix D in [21].

¹⁵This integral corresponds to the one given in eq. (5.4) in [30].

sets of mixed curvature-frame transitions, one for $N_- < 0$ and one for $N_- > 0$. There is a special orbit in the set for $\tilde{u} = \sqrt{2} - 1 \in (132)$ that is a straight line in the projection onto the plane $\Sigma_1 + \Sigma_2 + \Sigma_3 = 0$ in $(\Sigma_1, \Sigma_2, \Sigma_3)$ -space, described by $\Sigma_1 = -2(1 - \Sigma_3)$, $\Sigma_2 = 2 - 3\Sigma_3$, see Figure 4 (middle).

2.4. The orthogonally transitive subset \mathcal{OT}

The invariant \mathcal{OT} subset is defined by $R_1 = 0$. For this subset it is convenient to solve the constraint $\Sigma_1 + \Sigma_2 + \Sigma_3 = 0$ by introducing the following Misner parametrization adapted to the third spatial direction:

$$(25) \quad \Sigma_1 = \Sigma_+ + \sqrt{3}\Sigma_-, \quad \Sigma_2 = \Sigma_+ - \sqrt{3}\Sigma_-, \quad \Sigma_3 = -2\Sigma_+.$$

This implies that the equations in (1) lead to the following evolution equations

$$(26a) \quad \Sigma'_+ = 2(1 - \Sigma^2)\Sigma_+ + 2N_-^2 + \frac{3}{2}A^2,$$

$$(26b) \quad \Sigma'_- = 2(1 - \Sigma^2)\Sigma_- + \sqrt{3} [2N_-^2 - 2R_3^2 - \frac{1}{2}A^2],$$

$$(26c) \quad R'_3 = 2[1 - \Sigma^2 + \sqrt{3}\Sigma_-]R_3 - 4N_-A,$$

$$(26d) \quad N'_- = -2(\Sigma^2 + \Sigma_+ + \sqrt{3}\Sigma_-)N_- + 3R_3A,$$

$$(26e) \quad A' = -2(\Sigma^2 + \Sigma_+)A,$$

while the remaining constraints are given by

$$(27a) \quad 1 - \Sigma^2 - N_-^2 - A^2 = 0,$$

$$(27b) \quad 2R_3N_- + (\Sigma_+ + \sqrt{3}\Sigma_-)A = 0,$$

where $\Sigma^2 = \Sigma_+^2 + \Sigma_-^2 + R_3^2$.

The subset \mathcal{OT} contains the plane wave fixed points PW^\pm in (7). In the Misner variables (25), they become

$$(28) \quad \text{PW}^\pm := \left\{ \begin{array}{l} (\Sigma_-, A) = (1 + \Sigma_+)(\sqrt{3}, 2), \\ (R_1, R_3, N_-) = \pm \sqrt{-(3 + 4\Sigma_+)(1 + \Sigma_+)} (0, 1, 1) \end{array} \mid \Sigma_+ \in \left(-1, -\frac{3}{4}\right] \right\},$$

where $\Sigma_+ = \text{constant}$. In [31], it was shown that the \mathcal{OT} case admits a bounded (from above and below, since $|\Sigma_+| \leq 1$, $A \leq 1$) non-negative¹⁶ monotonic function, which in the present variables takes the form

$$(29) \quad Z := (1 + \Sigma_+)^2 - \frac{A^2}{4},$$

for which

$$(30) \quad Z' = 4(1 - \Sigma^2)Z.$$

Hence, the quantity Z is monotonically increasing, except when $Z = 0$ or $\Sigma^2 = 1$, where $Z = 0$ implies that $A = 2(1 + \Sigma_+)$, which characterizes the set $\overline{\text{PW}}^\pm = \text{PW}^\pm \cup \text{T}_3$, while $\Sigma^2 = 1$ implies that $N_- = A = 0$ due to the constraint (27a). The set $\Sigma^2 = 1$ consists

¹⁶Since Z is invariant under frame rotations in the $(1-2)$ -plane, it is not a coincidence that the proof that $Z \geq 0$ in [31] is also given in terms of such invariants.

of the union of the Kasner circle, K° (when $R_3 = 0$) and the single transition subset, \mathcal{T}_{R_3} (when $R_3 \neq 0$). It then follows from the stability properties of PW^\pm and K° that the α - and ω -limit set for these orbits respectively resides in $\overline{\text{PW}^\pm}$ and the stable sector $S_{\mathcal{OT}} := (312)$ of the Kasner circle K° , see Figure 5. Therefore, due to the monotonicity principle, see [63], this implies the following result:

Lemma 2.3. *The α -limit set for all \mathcal{OT} orbits resides in the set $\overline{\text{PW}^\pm}$, whereas the ω -limit set resides in the sector $S_{\mathcal{OT}} := (312)$ of the Kasner circle K° .*

We emphasize that the features of the monotone function Z do not prove if there are (or are not) any \mathcal{OT} orbits that possess the Taub point T_3 as its α -limit set. Alternatively, one can use the following non-negative bounded monotone function:

$$(31) \quad \bar{Z} := \frac{(1 + \Sigma_+)^2 - \frac{1}{4}A^2}{(1 + \Sigma_+)^2 + \frac{3}{4}A^2},$$

which satisfies

$$(32) \quad \bar{Z}' = 4(1 + \Sigma_+)\bar{Z}(1 - \bar{Z}).$$

The asymptotic subsets of the \mathcal{OT} subset are depicted in Figure 5. We finally note that the \mathcal{OT} subset presumably plays a similar role for the initial singularity attractor as the Bianchi type VII_0 subset does for Bianchi type IX.

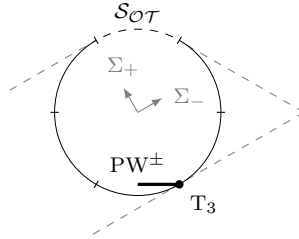


Figure 5: Projection of the asymptotic subsets within the \mathcal{OT} subset, which are described by the minima and maxima of the monotone function Z . The α -limits are contained in the closure of the plane wave fixed points $\overline{\text{PW}^\pm}$. It is unknown if there are \mathcal{OT} orbits that have T_3 as their α -limit. The ω -limits are contained in the (dashed) stable set $S_{\mathcal{OT}} \subseteq K^\circ$.

2.5. The hypersurface orthogonal subset \mathcal{HO}

The 2D hypersurface orthogonal invariant subset \mathcal{HO} with $n^\alpha_\alpha = 0$ (see e.g. [63]) occurs when $\Sigma_1 = R_3 = N_- = 0$. In Appendix A.4 we show that the dynamics in this invariant subset can be conveniently described by introducing $\sqrt{3}\Sigma_- := \Sigma_2 = -\Sigma_3$, which leads to

$$(33a) \quad \Sigma'_- = (1 - \Sigma_-^2)(2\Sigma_- + \sqrt{3}) - 2\sqrt{3}R_1^2,$$

$$(33b) \quad R'_1 = 2(1 - \Sigma_-^2 + \sqrt{3}\Sigma_-)R_1,$$

where $\Sigma^2 = \Sigma_-^2 + R_1^2$ while the constraint (2a) implies that $A^2 = 1 - \Sigma^2$.

Setting $R_1 = 0$ yields the invariant 1D diagonal shear and Fermi-propagated subset \mathcal{D} , on which

$$(34) \quad \Sigma'_- = (1 - \Sigma_-^2)(2\Sigma_- + \sqrt{3}).$$

This subset contains three fixed points: PW^0 with $\Sigma_- = -\sqrt{3}/2$ and the two Kasner fixed points with $\Sigma_- = \pm 1$, denoted by K_\pm° , where K_+° resides in sector (312) and has the following extended Kasner parameter value $\check{u} = -2 + \sqrt{3}$, while K_-° is in sector (213) with $\check{u} = -2 - \sqrt{3}$; both these Kasner points correspond to the frame-invariant Kasner parameter $u = 1 + \sqrt{3}$, which notably characterizes the double frame transition for which $\lambda_{R_1} = \lambda_{R_3}$, discussed in Section 2.2. Moreover, the invariant set \mathcal{D} with the evolution equation (34) is described by the two heteroclinic orbits $\text{PW}^0 \rightarrow \text{K}_\pm^\circ$, see Figure 6.

To obtain proofs about the two-dimensional dynamical system described by (33) with $R_1 > 0$, we use the following monotonic function (derived in Appendix A.4 using Hamiltonian techniques, where $v := -2/(3\sqrt{3})$ below is a boost in mini-superspace):

$$(35) \quad M := \frac{(1 - v\Sigma_-)^2}{[(1 - \Sigma^2)^9 R_1^5]^{\frac{2}{23}}},$$

which evolves according to

$$(36) \quad M' = \frac{27(\Sigma_- - v)^2}{23(1 - v\Sigma_-)} M,$$

where $1 - v\Sigma_- > 0$, since $|\Sigma_-| \leq 1$, due to the constraint (2a).

Hence M is monotonically increasing in the interior of the \mathcal{HO} state space, i.e. when $R_1 > 0$ and $\Sigma^2 = \Sigma_-^2 + R_1^2 < 1$. This implies that the fixed point RT, given by $(\Sigma_-, R_1) = (-2/(3\sqrt{3}), \sqrt{5}/(3\sqrt{3}))$, is a global minimum of M and thereby RT is a global source. Moreover, since $M \rightarrow \infty$, it follows that $R_1 = 0$ or $\Sigma^2 = 1$ when $\tau \rightarrow \infty$. The former consists of the invariant set \mathcal{D} , whereas the latter consists of a frame transition \mathcal{T}_{R_1} (and hence $A = 0$) given by $\text{K}_+^\circ \rightarrow \text{K}_-^\circ$. Incidentally, this heteroclinic orbit is part of a heteroclinic network on the boundary of the full state space, which plays an important role in the dynamics. In combination with the heteroclinic orbits on the boundary and the local fixed point analysis, M determines the global dynamics of the invariant \mathcal{HO} subset. In particular, PW^0 is a saddle that attracts a single interior heteroclinic orbit coming from RT, i.e. $\text{RT} \rightarrow \text{PW}^0$. Lastly, K_-° is a sink that attracts all interior orbits, except for the heteroclinic orbit $\text{RT} \rightarrow \text{PW}^0$, see Figure 6. We therefore obtain the following asymptotic characterization of the dynamics:

Lemma 2.4. *Apart from the fixed points, the three heteroclinic orbits $\text{K}_+^\circ \rightarrow \text{K}_-^\circ$, $\text{PW}^0 \rightarrow \text{K}_\pm^\circ$ on the boundary, and the heteroclinic orbit $\text{RT} \rightarrow \text{PW}^0$, all \mathcal{HO} orbits possess the following asymptotic structure: the α -limit set is the fixed point RT, whereas the ω -limit set is the fixed point K_-° .*

Due to the constraint $R_1^2 = 1 - \Sigma_-^2 - A^2$, one can alternatively use Σ_- and A as variables, which yields the dynamical system

$$(37a) \quad \Sigma'_- = -2\sqrt{3}(1 - \Sigma_-^2) + (2\Sigma_- + 3\sqrt{3})A^2,$$

$$(37b) \quad A' = -[2(1 - A^2) + \sqrt{3}\Sigma_-]A.$$

For the details of the dynamical systems features in the two representations (Σ_-, R_1) and (Σ_-, A) for the invariant subset \mathcal{HO} , see Figure 6.

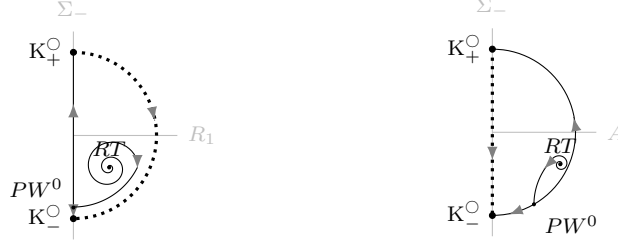


Figure 6: Schematic orbit structure of the 2D invariant set \mathcal{HO} using different variables. Note that the (dotted) heteroclinic orbit $K_+^O \rightarrow K_-^O$ is also contained in the set \mathcal{T}_{R_1} , see Figure 3. **Left:** the orbit structure resulting from the dynamical system (33) using the variables (Σ_-, R_1) . **Right:** the orbit structure resulting from the dynamical system (37) using (Σ_-, A) .

2.6. The $\mathcal{W}^s(\text{PW}^\pm)$ subset

Due to the linear analysis of PW^\pm (including PW^0) in (9), each of the fixed points on PW^\pm possesses a 1D local strong stable manifold and thereby attracts a single orbit from the interior generic 4D set. This amounts to a foliation of the 2D local center-stable manifold, $\mathcal{W}_{loc}^s(\text{PW}^\pm)$. We now make the following conjecture about the global properties of $\mathcal{W}_{loc}^s(\text{PW}^\pm)$, such as its global extensions and its boundary characterization.

Conjecture 2.5.

- (i) *The orbits in the manifold $\mathcal{W}^s(\text{PW}^\pm)$ originate from the local fixed point source RT , i.e., the α -limit set of all solutions in $\mathcal{W}^s(\text{PW}^\pm)$ is the fixed point RT , where the orbit $\text{RT} \rightarrow \text{PW}^0$ contained in the \mathcal{HO} subset divides $\mathcal{W}^s(\text{PW}^\pm)$ into two parts: $\text{RT} \rightarrow \text{PW}^+$ and $\text{RT} \rightarrow \text{PW}^-$.*
- (ii) *The boundaries of the two parts $\text{RT} \rightarrow \text{PW}^\pm$, and thereby the whole subset $\mathcal{W}^s(\text{PW}^\pm)$, are given by two heteroclinic orbits $\text{RT} \rightarrow \text{T}_3$, where one orbit is approaching T_3 from the positive R_3, N_- direction and the other from the negative R_3, N_- direction, due to the discrete symmetry $(R_3, N_-) \mapsto -(R_3, N_-)$.*

3. Induced discrete dynamics

It is generally believed that the attractor \mathcal{A} that describes the generic behaviour in the vicinity of the initial singularity resides on the union of the Bianchi type I Kasner subset, \mathcal{K} , and the Bianchi type II subset, \mathcal{B}_{II} , which leads to the following conjecture:

Conjecture 3.1. $\mathcal{A} = \mathcal{K} \cup \mathcal{B}_{\text{II}} = \text{K}^O \cup \mathcal{T}_{R_1} \cup \mathcal{T}_{R_3} \cup \mathcal{T}_{R_1 R_3} \cup \mathcal{T}_{N_-} \cup \mathcal{T}_{R_1 N_-}$.

Motivated by the numerical investigations in [30], which suggests that multiple transitions become increasingly rare and thus only single transitions play an asymptotical role, the following stronger conjecture was introduced in [30]:¹⁷

Conjecture 3.2. $\mathcal{A} = \text{K}^O \cup \mathcal{T}_{R_1} \cup \mathcal{T}_{R_3} \cup \mathcal{T}_{N_-}$.

¹⁷A conjecture which is also supported by the analysis in [21], which in turn is related to the configuration space cosmological billiard approach in [12].

To prove these attractor conjectures, if true, one might have to proceed as in the attractor theorem for Bianchi type IX, see [53, 24]. As a first step, one would need to obtain a monotonic function that shows that the attractor resides on a union of (or possibly some of) the 3D subsets, as is the case for the toy model described in Appendix A.1. Then one needs to obtain the asymptotic structures of these subsets (and possibly perturbations thereof), as illustrated by the Lemmata 2.1, 2.2, 2.3, 2.4 and also the Conjecture 2.5, with the aim of excluding certain subsets.

For example, since RT is an unstable fixed point, it will not attract any solutions in the state space. Similarly, note that the \mathcal{HO} subset consists of a 2D submanifold of the 4D unstable manifold of RT and thus orbits in the interior of \mathcal{HO} can not attract any solution in the state space, although the heteroclinic boundary orbits $K_+^\circ \rightarrow K_-^\circ$ and $PW^0 \rightarrow K_\pm^\circ$ can not a priori be excluded as part of the ω -limit of a generic type VI $_{-1/9}$ solution. Moreover, if Conjecture 2.5 is true, and the α -limit set of all non-PW $^\pm$ solutions in the closure of $\mathcal{W}^s(PW^\pm)$ is the fixed point RT, then we can also exclude all the heteroclinic orbits within this set from \mathcal{A} . However, the conjectures require us to exclude the orbit $PW^0 \rightarrow K_\pm^\circ$, as well as the whole interior \mathcal{OT} subset from \mathcal{A} , which contains the arc of plane wave fixed points, PW $^\pm$, since both conjectures require that $\lim_{\tau \rightarrow \infty} A = 0$.

That $\lim_{\tau \rightarrow \infty} A = 0$ actually happens is motivated by the linear analysis of equation (1) at K° since this yields $A' = -3(1 - p_3)A = -\frac{3}{f(\bar{u})}A$, which implies that $\lim_{\tau \rightarrow +\infty} A = 0$ everywhere on K° , except at the Taub point T_3 where $p_3 = 1$.

To provide a first step analyzing the regions of instability of the variable A , we rewrite equation (1g) using the Misner variables in (25), i.e.,

$$(38) \quad \Sigma_1 = \Sigma_+ + \sqrt{3}\Sigma_-, \quad \Sigma_2 = \Sigma_+ - \sqrt{3}\Sigma_-, \quad \Sigma_3 = -2\Sigma_+,$$

which yields

$$(39) \quad A' = -2 \left[\left(\Sigma_+ + \frac{1}{2} \right)^2 + \Sigma_-^2 + R_1^2 + R_3^2 - \frac{1}{4} \right] A.$$

This implies that the only region where A increases is in a four dimensional ball of radius 1/2 centered at $(\Sigma_+, \Sigma_-, R_1, R_3) = (-\frac{1}{2}, 0, 0, 0)$, where a projection of this ball onto the plane $\Sigma_1 + \Sigma_2 + \Sigma_3 = 0$ in $(\Sigma_1, \Sigma_2, \Sigma_3)$ -space is given in Figure 7. Alternatively, we note that A is increasing if

$$(40) \quad N_-^2 + A^2 > 1 + \Sigma_+,$$

where we have used the Gauss constraint $1 = \Sigma^2 + N_-^2 + A^2$ in connection with (39).

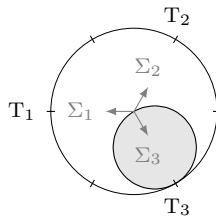


Figure 7: The shaded region is the projection onto the plane $\Sigma_1 + \Sigma_2 + \Sigma_3 = 0$ in $(\Sigma_1, \Sigma_2, \Sigma_3)$ -space of the region where A increases. Note that this ball is tangential to the Taub point T_3 .

Motivated by the above attractor conjectures and the new generation of proofs for Bianchi type VIII and IX, which uses the properties of the Bianchi type I and II heteroclinic network [2, 37, 38, 3], we now first consider the discrete dynamics induced by the Bianchi type I and II frame and curvature transition boundary subsets in Bianchi type VI_{-1/9}.

3.1. Kasner circle transition maps

We first note that the single frame transitions \mathcal{T}_{R_1} and \mathcal{T}_{R_3} induce a map of the Kasner circle K° , which maps the α -limit set to the ω -limit set of each heteroclinic orbit. Using the same nomenclature to denote such maps, they are given by the extended Kasner parameter \check{u} according to

$$(41a) \quad \mathcal{T}_{R_1}(\check{u}) := \frac{1}{\check{u}}, \quad \text{for } \check{u} \in (-1, 1),$$

$$(41b) \quad \mathcal{T}_{R_3}(\check{u}) := -(1 + \check{u}), \quad \text{for } \check{u} \in \left(-\infty, -\frac{1}{2}\right).$$

We then note that for any point $\check{u} \in (-1, -\frac{1}{2})$, which corresponds to sector (321) and thereby the multivalued region $\mathbf{A}_{R_1 R_3}^-$, the frame transitions commute after three iterates, i.e. $\mathcal{T}_{R_1} \circ \mathcal{T}_{R_3} \circ \mathcal{T}_{R_1}(\check{u}) = -\frac{\check{u}}{1+\check{u}} = \mathcal{T}_{R_3} \circ \mathcal{T}_{R_1} \circ \mathcal{T}_{R_3}(\check{u})$, see Figure 8 (left). The corresponding orbits form the boundary of the double frame transitions, and hence uniquely defines the Kasner circle double frame transition map,

$$(42) \quad \mathcal{T}_{R_1 R_3}(\check{u}) := -\frac{\check{u}}{1 + \check{u}}, \quad \text{for } \check{u} \in \left(-1, -\frac{1}{2}\right).$$

The effect of a double frame transition is to interchange the first and third directions while Σ_2 is unchanged, i.e. $(\Sigma_2)_- = 3(p_2)_- - 1 = 3(p_2)_+ - 1 = (\Sigma_2)_+$.

Similarly, the single curvature transitions \mathcal{T}_{N_-} induce a map of the Kasner circle K° , which can be expressed by the extended Kasner parameter \check{u} as follows:

$$(43) \quad \mathcal{T}_{N_-}(\check{u}) := -\check{u}, \quad \text{for } \check{u} \in (0, +\infty).$$

For any point $\check{u} \in (0, 1)$, which corresponds to sector (132) and thereby the multivalued region $\mathbf{A}_{R_1 N_-}^-$, note that a curvature transition \mathcal{T}_{N_-} and a frame transition \mathcal{T}_{R_1} commute after two iterates, i.e. $\mathcal{T}_{R_1} \circ \mathcal{T}_{N_-}(\check{u}) = -\frac{1}{\check{u}} = \mathcal{T}_{N_-} \circ \mathcal{T}_{R_1}(\check{u})$, see Figure 8 (right), which uniquely defines the mixed curvature-frame transition map,

$$(44) \quad \mathcal{T}_{R_1 N_-}(\check{u}) := -\frac{1}{\check{u}}, \quad \text{for } \check{u} \in (0, 1).$$

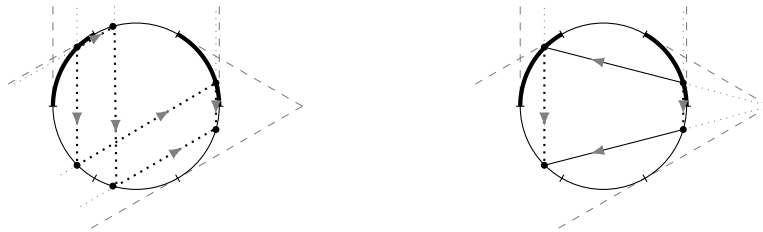


Figure 8: Left: Commutation of the frame transitions, $\mathcal{T}_{R_1} \circ \mathcal{T}_{R_3} \circ \mathcal{T}_{R_1} = \mathcal{T}_{R_3} \circ \mathcal{T}_{R_1} \circ \mathcal{T}_{R_3}$, which defines a unique double frame transition map, $\mathcal{T}_{R_1 R_3}$. **Right:** Commutation of the curvature and frame transitions, $\mathcal{T}_{R_1} \circ \mathcal{T}_{N_-} = \mathcal{T}_{N_-} \circ \mathcal{T}_{R_1}$, which defines a unique mixed curvature-frame transition map $\mathcal{T}_{R_1 N_-}$.

Recall that the unstable modes trigger transitions from each corresponding sector and note that the stable modes are complementary to those modes, see Figure 2, and that this serves as the foundation for the Bianchi type I and II heteroclinic network. There are two possible single transitions in the sectors (321) and (132). To obtain unique maps, we view the 1-parameter sets of heteroclinic orbits at each point on K° associated with $\mathcal{T}_{R_1R_3}$ and $\mathcal{T}_{R_1N_-}$, including their boundaries, as equivalence classes, and use the maps (42) and (44). This is in contrast to the iterated function system analysis developed in [36] and the description of Kasner epochs using symbolic dynamics in [27]. Note that the column for the Domain in Table 2 then covers all the sectors of K° , where the unique map for each sector is given in Table 2.

Map	Image of \check{u}	Domain	Range
\mathcal{T}_{R_3}	$-(1 + \check{u})$	$(-\infty, -1) \in (213) \cup (231)$	$(0, \infty) \in (123) \cup (132)$
$\mathcal{T}_{R_1R_3}$	$-\frac{\check{u}}{1+\check{u}}$	$(-1, -\frac{1}{2}) \in (321)$	$(1, \infty) \in (123)$
\mathcal{T}_{R_1}	$\frac{1}{\check{u}}$	$(-\frac{1}{2}, 0) \in (312)$	$(-\infty, -2) \in (213)$
$\mathcal{T}_{R_1N_-}$	$-\frac{1}{\check{u}}$	$(0, 1) \in (132)$	$(-\infty, -1) \in (213) \cup (231)$
\mathcal{T}_{N_-}	$-\check{u}$	$(1, \infty) \in (123)$	$(-\infty, -1) \in (213) \cup (231)$

Table 2: Unique maps for each sector. For example, the single curvature transitions are given as follows: any $\check{u} \in (1, \infty)$, which parametrizes sector (123), yields the map $\mathcal{T}_{N_-}(\check{u}) = -\check{u} \in (-\infty, -1)$, which parametrizes sectors (213), on which $\check{u} \in (-\infty, -2)$, and (231), for which $\check{u} \in (-2, -1)$.

Even though this has advantages, this also results in disadvantages, e.g., considering only multiple transitions omits some heteroclinic chains. Moreover, there is no mathematical reason for why the multiple transitions should play a more significant asymptotic role than the single transitions in the asymptotic dynamics — the stronger of the above two attractor conjectures even asymptotically rules out multiple transitions!

3.2. Frame-invariant discrete dynamics

Frame transitions do not change the frame-invariant Kasner parameter u ; this only happens for the curvature transitions \mathcal{T}_{N_-} and $\mathcal{T}_{R_1N_-}$, which both yield the change

$$(45) \quad u_+ = \begin{cases} u_- - 1 & \text{if } u_- \in [2, \infty), \\ \frac{1}{u_- - 1} & \text{if } u_- \in [1, 2], \end{cases}$$

which is known as the *BKL map*, see [5]. A sequence of transitions corresponds to an iteration of (45). The frame-invariant curvature transition from u_i to u_{i+1} , $i = 0, 1, 2, \dots$,

$$(46) \quad u_i \xrightarrow{\textit{i}^{\textit{th}} \textit{ curvature transition}} u_{i+1},$$

is thereby described by the BKL map,

$$(47) \quad u_{i+1} = \begin{cases} u_i - 1 & \text{if } u_i \in [2, \infty), \\ \frac{1}{u_i - 1} & \text{if } u_i \in [1, 2]. \end{cases}$$

The information contained in this map suffices to represent the collection of all transition orbits (as a whole) that undergo a single or mixed curvature-frame transition.

In a sequence $(u_i)_{i \in \mathbb{N}_0}$ that is generated by the BKL map (47), each Kasner state u_i is called a frame-invariant *Kasner epoch*. A given sequence, $(u_i)_{i \in \mathbb{N}_0}$ of frame-invariant Kasner epochs possesses a natural partition into pieces called (frame-invariant) *Kasner eras* based on the properties of (47), see [5]:

$$(48) \quad \{u_0, u_1, u_2, \dots\} = \underbrace{\{u_0^0, \dots, u_f^0\}}_{\text{Initial era}} \underbrace{\{u_0^1, \dots, u_f^1\}}_{1^{\text{st}} \text{ era}} \underbrace{\{u_0^2, \dots, u_f^2\}, \dots}_{2^{\text{nd}} \text{ era}} \underbrace{\{u_0^j, \dots, u_f^j\}, \dots}_{j^{\text{th}} \text{ era}},$$

where $u_0^0 = u_0$ and where each j^{th} era begins with the largest Kasner epoch value u_0^j in the era followed by a finite monotonically decreasing sequence of frame-invariant Kasner parameters, obtained from $u_{k+1}^j = u_k^j - 1$, until it reaches the final smallest value $u_f^j \in (1, 2)$, which in turn yields the initial Kasner parameter value $u_0^{j+1} = 1/(u_f^j - 1)$ of the next $(j + 1)^{\text{th}}$ era. For example,

$$(49) \quad \underbrace{5.29 \rightarrow 4.29 \rightarrow 3.29 \rightarrow 2.29 \rightarrow 1.29}_{\text{Initial era}} \rightarrow \underbrace{3.44 \rightarrow 2.44 \rightarrow 1.44}_{1^{\text{st}} \text{ era}} \rightarrow \underbrace{2.27 \rightarrow 1.27}_{2^{\text{nd}} \text{ era}} \rightarrow \dots$$

Following [5, 34], we decompose each u_0^j into its integer, $\lfloor u_0^j \rfloor \in \mathbb{N}$, and fractional, $\{u_0^j\} \in (0, 1)$, parts. Hence, in the j^{th} era, the Kasner parameter u_0^j denotes the maximal value of the parameter among the $\lfloor u_0^j \rfloor$ Kasner epochs in the j^{th} era, which decreases $\lfloor u_0^j \rfloor - 1$ times by 1 until its minimal value, $u_f^j = 1 + \{u_0^j\}$. This induces the following definition, called the (frame-invariant) *Era map*,

$$(50) \quad u_0^j \mapsto u_0^{j+1} = \frac{1}{\{u_0^j\}},$$

which thereby generates a sequence $(u_0^j)_{j \in \mathbb{N}_0}$. It is known that the transformation (50) is associated with exponential instability: the distance between two sufficiently close points grows exponentially with the number of iterations j , see [34].

Next, we give an interpretation of the Kasner parameter u and the map (47) in terms of continued fraction representations. Before doing so, however, we introduce the following notation for the set of frame-invariant Kasner parameter values in the j^{th} era:

$$(51) \quad \mathbb{E}^j := \{u_0^j, \dots, u_f^j\}.$$

Now, consider a Kasner sequence $\{u_0, u_1, \dots\}$, partitioned into different eras according to (48). The initial Kasner epoch value, which is the first epoch in the initial era, i.e. $u_0 = u_0^0 \in \mathbb{R}$, is represented by the continued fraction:

$$(52) \quad u_0 = k_0 + \frac{1}{k_1 + \frac{1}{k_2 + \dots}},$$

where $\lfloor u_0 \rfloor = k_0$ and $\{u_0\} = [0; k_1, k_2, k_3, \dots]$. According to the BKL map (47), the value u_0 decreases by 1 a total of $k_0 - 1$ times until it reaches a final value $u_f^0 \in (1, 2)$. The BKL map (47) then maps the final epoch of the initial era to the initial epoch of the 1^{st} era, $u_f^0 \in \mathbb{E}^0 \mapsto u_0^1 = 1/(u_f^0 - 1) \in \mathbb{E}^1$, which leads to the continued fraction representation

$$(53) \quad u_0^1 = k_1 + \frac{1}{k_2 + \frac{1}{k_3 + \dots}} = [k_1; k_2, k_3, k_4, \dots].$$

The *Era map* is thereby simply a shift to the left in the continued fraction expansion,

$$(54) \quad u_0^j = [k_j; k_{j+1}, k_{j+2}, \dots] \mapsto u_0^{j+1} = [k_{j+1}; k_{j+2}, k_{j+3}, \dots].$$

It thus follows that the Kasner sequence $(u_i)_{i \in \mathbb{N}_0}$, generated by $u_0 = [k_0; k_1, k_2, \dots]$, amounts to the following concatenation of maps in terms of continued fractions:

$$(55) \quad \begin{aligned} u_0 = u_0^0 &= [k_0; k_1, k_2, \dots] \rightarrow [k_0 - 1; k_1, k_2, \dots] \rightarrow \dots \rightarrow [1; k_1, k_2, \dots] \\ &\rightarrow u_0^1 = [k_1; k_2, k_3, \dots] \rightarrow [k_1 - 1; k_2, k_3, \dots] \rightarrow \dots \rightarrow [1; k_2, k_3, \dots] \\ &\rightarrow u_0^2 = [k_2; k_3, k_4, \dots] \rightarrow [k_2 - 1; k_3, k_4, \dots] \rightarrow \dots \end{aligned}$$

Below we relate properties of Kasner sequences to properties of u_0 by inferring these from the continued fraction expansion of u_0 . We are particularly interested in generic dynamics of (55), but note that genericity is a delicate issue since there are several notions of genericity, such as measure theoretical genericity (e.g. the Lebesgue measure) or topological genericity (e.g. the Baire measure).

- (i) The initial Kasner parameter is a *rational number*, $u_0 \in \mathbb{Q}$, if, and only if, its continued fraction representation is finite:

$$(56) \quad u_0 = [k_0; k_1, k_2, \dots, k_n],$$

such that $k_n > 1$; [57, Lemma 4B]. The Kasner sequence is thereby finite with $n + 1$ eras where the last era begins with k_n . At the end of the last era the Kasner parameter reaches $u_f^n = 1$, which subsequently terminates the recursion (47) at a Taub state/epoch. Even though \mathbb{Q} is a dense set in \mathbb{R} , it is a set of Lebesgue measure zero and thus this case is non-generic.

On the other hand, the irrational numbers, $\mathbb{R} \setminus \mathbb{Q}$, consist of a dense set of full Lebesgue measure in \mathbb{R} . We will now describe several interesting subcases, where genericity is a subtle issue for some of them.

- (ii) The initial Kasner parameter u_0 is a *badly approximable irrational number*¹⁸ if, and only if, its continued fraction representation is bounded, i.e.

$$(57) \quad u_0 = [k_0; k_1, k_2, k_3, \dots] \quad \text{with} \quad k_i \leq K, \quad \forall i = 0, 1, 2, \dots$$

for some constant $K > 0$, see [57, Theorem 5F]. Consequently, the Kasner sequence $(u_i)_{i \in \mathbb{N}_0}$ is bounded, i.e., $u_i \leq (K + 1), \forall i \in \mathbb{N}_0$. The set of badly approximable irrational numbers is a set of Lebesgue measure zero (see [57, Page 60]), which thereby is a non-generic set in a measure theoretic sense, but it has full Hausdorff dimension that equals 1, see [56]. Of particular interest is the following subcase:

- (ii.1) The initial Kasner parameter u_0 is a *quadratic irrational number*¹⁹ if, and only if, its continued fraction representation possess a periodic tail, i.e., when

$$(58) \quad u_0 = [k_0; k_1, \dots, k_n, \overline{k_{n+1}, \dots, k_{n+p}}],$$

¹⁸A number $u_0 \in \mathbb{R} \setminus \mathbb{Q}$ is called a *badly approximable irrational number* if there is a constant $c > 0$ such that for all rational numbers, p/q , we have that $|u_0 - p/q| > c/q^2$.

¹⁹A *quadratic irrational number* (quadratic surd) is an algebraic number of degree 2, i.e., an irrational solution of a quadratic equation with integer coefficients. In particular, such a solution can be written as $q_1 + \sqrt{q_2}$, where $q_1 \in \mathbb{Q}$ and where $q_2 \in \mathbb{Q}$ is not a perfect square, i.e., $\sqrt{q_2} \notin \mathbb{Q}$.

where k_1, \dots, k_n represents a preperiodic piece and $\overline{k_{n+1}, \dots, k_{n+p}}$ is repeated ad infinitum, see [57, Theorem 6A], where $\overline{k_{n+1}, \dots, k_{n+p}}$ yields both a periodic Kasner sequence with the period $k_{n+1} + \dots + k_{n+p}$ and a periodic sequence of eras with the period p . If $u_0 = q_1 + \sqrt{q_2} > 1$ is a quadratic irrational number such that $q_1 - \sqrt{q_2} \in (-1, 0)$, then the continued fraction is purely periodic without any preperiodic piece, i.e. $u_0 = [\overline{k_1, \dots, k_p}]$. Since the set of algebraic numbers of degree two is a countable set, this case is also non-generic.

- (iii) If the initial Kasner parameter u_0 is a *well approximable irrational number*²⁰, then the partial quotients k_i in the continued fraction representation

$$(59) \quad u_0 = [k_0; k_1, k_2, k_3, \dots]$$

are unbounded. In particular, we can construct a diverging subsequence of $(k_i)_{i \in \mathbb{N}_0}$ and hence such sequences come arbitrarily close to a Taub state, which corresponds to $u = \infty$. Since this is the complementary set of badly approximable irrational numbers (which is of Lebesgue measure zero), this set is of full Lebesgue measure. This is the generic case, in terms of Lebesgue measure, and hence generically the Kasner sequence $(u_i)_{i \in \mathbb{N}_0}$ is infinite and unbounded. We consider three subcases:

- (iii.1) If $u_0 \in (1, 2)$ is a *very well approximable irrational number*²¹, then there exists a constant $c > 0$ such that the partial quotients k_i in the continued fraction representation for infinitely many integers n obey the following inequality:

$$(60) \quad \log(1 + k_{n+1}) \geq c \sum_{i=1}^n \log(1 + k_i),$$

see [35, Corollary 7.2]. The set of such u_0 has Lebesgue measure zero, whereas its Hausdorff dimension is equal to 1. Thus this case is not generic in the sense of Lebesgue measure.

- (iii.2) When u_0 is a *Liouville number*²², then the set of such u_0 can also be characterized by the partial quotients k_i in the continued fraction representation as follows: for all $c > 0$ there are infinitely many integers n such that the inequality (60) holds; see [35, Corollary 2.8]. The set of Liouville numbers is an uncountable dense set of the real numbers, such that both its Lebesgue measure and Hausdorff dimension are equal to zero. Thus this case is not generic in terms of Lebesgue measure, but there exists a measure μ , invariant with respect to the Gauss map, which yields full measure of the Liouville numbers, see [35, Theorem 4.5].

- (iii.3) The works [3] and [50] considered Bianchi type VIII and IX and introduced certain conditions on the coefficients of the continued fraction expansion of

²⁰A number $u_0 \in \mathbb{R} \setminus \mathbb{Q}$ is called *well approximable irrational number* if it is not a badly approximable irrational number.

²¹A number $u_0 \in \mathbb{R} \setminus \mathbb{Q}$ is called *very well approximable irrational number* if for some integer $n > 0$, there are two integers p, q with $q > 1$ such that $|u_0 - p/q| < 1/q^n$.

²²A number $u_0 \in \mathbb{R}$ is called *Liouville number* if for every integer $n > 0$ there are two integers p, q with $q > 1$ such that $0 < |u_0 - p/q| < 1/q^n$. Intuitively, Liouville numbers are ‘almost rational’, and can thus be very well approximated by sequences of rational numbers.

u_0 , which may also be of interest for Bianchi type VI $_{-1/9}$. If u_0 satisfies the moderate growth condition

$$(61) \quad k_{n+4}^A = o_{n \rightarrow \infty} \left(\sum_{i=1}^n k_i^5 \right),$$

then this set of u_0 has full Lebesgue measure and possesses stable manifolds of positive Lebesgue measure in the state space considered in [3]. The work [50] describes a different set of full Lebesgue measure consisting of values of u_0 that satisfies a subpolynomial bound on the coefficients of its continued fraction expansion, which is different than imposing (61) and (60).

Note that although all these sets of continued fractions and bounds are different (possibly with some intersections), they have a common feature: they are conditions that bound the coefficients of a continued fraction expansion by the previous coefficients.

3.3. From frame-invariant Kasner sequences to networks of heteroclinic chains

In the state space of (1), (2) it follows straightforwardly that each frame-invariant Kasner epoch, described by a Kasner parameter $u \neq 1, \infty$, corresponds to the invariant set given by the closure of the double frame transitions, $\overline{\mathcal{T}}_{R_1 R_3}(\check{u})$, originating from the fixed point with $\check{u} = -u/(1+u)$ in sector (321), see Table 1 and Figure 3. The invariant set $\overline{\mathcal{T}}_{R_1 R_3}(\check{u})$ consists of:

- (i) Six fixed points on K° , one in each sector, given by $\check{u} = \check{u}(u)$ according to Table 1.
- (ii) Two equivalence classes, related by $R_3 \rightarrow -R_3$, of heteroclinic single frame transition chains, given by $\mathcal{T}_{R_1} \circ \mathcal{T}_{R_3} \circ \mathcal{T}_{R_1}(\check{u})$ and $\mathcal{T}_{R_3} \circ \mathcal{T}_{R_1} \circ \mathcal{T}_{R_3}(\check{u})$, where each heteroclinic chain connects four fixed points on K° according to (see the figure to the right in Figure 3)

$$\begin{aligned} (321) \cdots \blacktriangleright (312) \cdots \blacktriangleright (213) \cdots \blacktriangleright (123), \\ (321) \cdots \blacktriangleright (231) \cdots \blacktriangleright (132) \cdots \blacktriangleright (123), \end{aligned}$$

respectively, where $\check{u}(u)$ for the different sectors are given in Table 1. Note that both types of heteroclinic chains connect the common first and final fixed points in sector (321), where $\check{u} = -u/(1+u)$, and sector (123), where $\check{u} = u$, respectively, which reflects the commuting property $\mathcal{T}_{R_1} \circ \mathcal{T}_{R_3} \circ \mathcal{T}_{R_1}(\check{u}) = \mathcal{T}_{R_3} \circ \mathcal{T}_{R_1} \circ \mathcal{T}_{R_3}(\check{u})$, $\check{u} = -u/(1+u)$, illustrated to the left in Figure 8.

- (iii) An equivalence class, related by $R_3 \rightarrow -R_3$, of 1-parameter sets of heteroclinic double frame transition orbits $\overline{\mathcal{T}}_{R_1 R_3}(\check{u})$, connecting the fixed point $\check{u} = -u/(1+u)$ in sector (321) with that in sector (123) given by $\check{u} = u$, where the heteroclinic chains in (ii) form the boundary of $\overline{\mathcal{T}}_{R_1 R_3}(\check{u})$.

Describing the heteroclinic network corresponding to a frame-invariant Kasner sequence $\{u_0, u_1, u_2, \dots\}$, which yields an entangled set of heteroclinic chains by projecting orbits onto the plane $\Sigma_1 + \Sigma_2 + \Sigma_3 = 0$ in $(\Sigma_1, \Sigma_2, \Sigma_3)$ -space, becomes quite complicated already after a few Kasner epochs. For this reason we will introduce a simplifying representation, which emphasizes that such a heteroclinic network is a directed graph, where the vertices

are points on K° while the edges are the heteroclinic orbits connecting them, with no loops (i.e. self-connections). This representation is obtained by arranging the six fixed points $\check{u} = \check{u}(u)$ by means of the heteroclinic single transition chains in (ii) above so that they form a hexagon, illustrating the commuting feature $\mathcal{T}_{R_1} \circ \mathcal{T}_{R_3} \circ \mathcal{T}_{R_1}(\check{u} \in (321)) = \mathcal{T}_{R_3} \circ \mathcal{T}_{R_1} \circ \mathcal{T}_{R_3}(\check{u} \in (321))$, while the double frame transition orbits $\mathcal{T}_{R_1 R_3}(\check{u} \in (321))$ in (iii) are represented by an arrow inside the hexagon, symbolizing that the hexagon chains in (ii) form the boundary of $\mathcal{T}_{R_1 R_3}(\check{u} \in (321))$, see Figure 9, see also Figure 3 (right).



Figure 9: Graph representation of a heteroclinic network corresponding to a frame-invariant Kasner parameter $u \neq 1, \infty$, obtained from $\overline{\mathcal{T}}_{R_1 R_3}(\check{u})$, where $\check{u} = \check{u}(u) = -u/(1+u) \in (321)$. **Left:** The six fixed points \check{u} in the different sectors, given by \check{u} in Table 1, are arranged as the vertices of a hexagon-shaped graph, where the edges are given by the heteroclinic chains of single frame transition, $\mathcal{T}_{R_3} \circ \mathcal{T}_{R_1} \circ \mathcal{T}_{R_3}(\check{u} \in (321))$ and $\mathcal{T}_{R_1} \circ \mathcal{T}_{R_3} \circ \mathcal{T}_{R_1}(\check{u} \in (321))$, represented by thin dotted arrows. The family of double frame transition orbits, $\mathcal{T}_{R_1 R_3}(\check{u} \in (123))$, are represented by a bold dotted arrow inside the hexagon. **Right:** To avoid clutter when representing Kasner sequences as sequences of hexagons, the sector notation for the fixed points is omitted and replaced with dots.

The map (45) has two different cases for a given frame-invariant Kasner parameter u_- : when $u_- \in (2, \infty)$ an era continues according to $u_+ = u_- - 1$, while when $u_- \in (1, 2)$ the era changes according to $u_+ = 1/(u_- - 1)$. These two intervals, $(1, 2) \cup (2, \infty)$, partition each sector on K° into two disjoint parts. For example, sector (132) is divided into $(132)_f$ with $\check{u}_- = 1/u_- \in (\frac{1}{2}, 1)$, corresponding to $u_- \in (1, 2)$, and its open complement $(132)_c$ with $\check{u}_- = 1/u_- \in (0, \frac{1}{2})$ for which $u_- \in (2, \infty)$, see Table 1 and Figure 2.

In the hexagon representation, the two epochs u_- and u_+ correspond to two hexagons, where the two different rules connecting these two Kasner states, depending on the range of u_- , amount to connecting the two hexagons in two different ways:

- **No era change:** A change of Kasner epochs without a change of Kasner era takes place when $u_- \in (2, \infty)$, for which the frame-invariant BKL map (45) yields $u_+ = u_- - 1$. This corresponds to connecting the two hexagon graphs with u_- and u_+ according to:
 - (i) The single curvature transition $\mathcal{T}_{N_-}(\check{u}_-)$, $\check{u}_- = u_- \in (2, \infty) = (123)_c$, from sector $(123)_c$ to sector (213).
 - (ii) The single curvature transition $\mathcal{T}_{N_-}(\check{u}_-)$, where $\check{u}_- = 1/u_- \in (0, \frac{1}{2}) = (132)_c$, from sector $(132)_c$ to sector (312).
 - (iii) The mixed curvature-frame transitions $\mathcal{T}_{R_1 N_-}(\check{u}_-)$, where $\check{u}_- = 1/u_- \in (0, \frac{1}{2}) = (132)_c$, from sector $(132)_c$ to sector (213),

as in Figure 10 (left), see also Figure 4 (right). The heteroclinic chain given by $(321) \cdots \blacktriangleright (231) \cdots \blacktriangleright (132) \cdots \blacktriangleright (123)$, the heteroclinic orbit $(321) \cdots \blacktriangleright (312)$, and the double frame transition heteroclinics $(321) \cdots \blacktriangleright (123)$ in the hexagon associated with

u_+ are not part of any heteroclinic chain that originates from the hexagon corresponding to u_- . Therefore we say that the fixed points \check{u}_+ in sectors (321), (231), (132) and the heteroclinic orbits that originate from them are *isolated*. Figure 10 (left).

- **Era change:** A change of a Kasner era takes place when $u_- \in (1, 2)$, where the BKL map (45) yields $u_+ = 1/(u_- - 1)$. This corresponds to connecting the two hexagon graphs corresponding to u_- and u_+ , respectively according to:

- The single curvature transition $\mathcal{T}_{N_-}(\check{u}_- = u_-)$, $\check{u}_- = u_- \in (1, 2) = (123)_f$, from sector (123)_f to sector (231).
- The single curvature transition $\mathcal{T}_{N_-}(\check{u}_-)$, $\check{u}_- = 1/u_- \in (\frac{1}{2}, 1) = (132)_f$, from sector (132)_f to sector (321).
- The mixed curvature-frame transitions $\mathcal{T}_{R_1 N_-}(\check{u}_-)$, where $\check{u}_- = 1/u_- \in (\frac{1}{2}, 1) = (132)_f$, from sector (132)_f to sector (231),

as illustrated in Figure 10 (right), see also Figure 4 (middle). Note that this case does not yield any isolated structure.

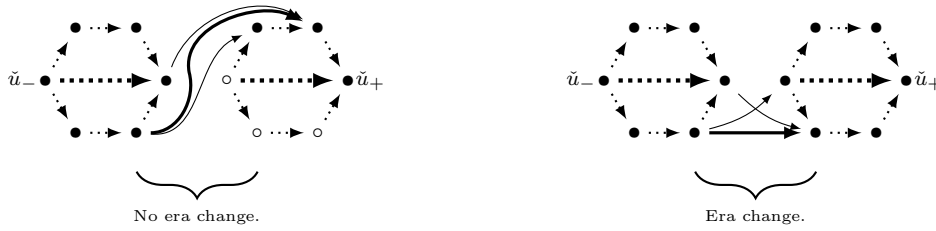


Figure 10: The Kasner parameters u_- and u_+ yield two hexagons using the graph representations in Figure 9. The BKL map (45), $u_- \mapsto u_+$, yields two rules for how to connect such hexagons through heteroclinic orbits. We represent single curvature (mixed curvature-frame) transitions with thin (thick) solid arrows. **Left:** Representation of the heteroclinic connections between the hexagons with u_- and u_+ when there is no era change, i.e. when $u_- \in (2, \infty)$ and $u_+ = u_- - 1$. Note that in the hexagon to the right, corresponding to u_+ , there are fixed points (and thereby heteroclinic orbits originating from them) that are not connected to any point in the leftmost hexagon associated with u_- . This yields an *isolated* structure, and for this reason, we depict such fixed points with hollow circles. **Right:** Representation of the heteroclinic orbit connections between the hexagons with u_- and u_+ when there is an era change, i.e. when $u_- \in (1, 2)$ and $u_+ = 1/(u_- - 1)$. Note that this case does not yield any isolated structure.

Next we consider frame-invariant Kasner sequences $(u_i)_{i \in \mathbb{N}_0}$ partitioned into (frame-invariant) Kasner eras according to (48), which we for convenience repeat:

$$(62) \quad \{u_0, u_1, u_2, \dots\} = \underbrace{\{u_0^0, \dots, u_f^0\}}_{\text{Initial era}}, \underbrace{\{u_0^1, \dots, u_f^1\}}_{1^{\text{st}} \text{ era}}, \underbrace{\{u_0^2, \dots, u_f^2\}}_{2^{\text{nd}} \text{ era}}, \dots, \underbrace{\{u_0^j, \dots, u_f^j\}}_{j^{\text{th}} \text{ era}}, \dots,$$

where $u_0^0 = u_0$. Due to the definition of the BKL map (47), points within (132)_f correspond to the final values u_f^j for all $j = 0, 1, 2, \dots$ in all eras, whereas points within (132)_c correspond to all other Kasner parameter values, not being a final era value, i.e. $\mathbb{E}^j \setminus \{u_f^j\}$ for all $j = 0, 1, 2, \dots$ (recall (51), which introduced the notation \mathbb{E}^j for the number of Kasner epochs, given by $[u_0^j]$, for the j^{th} era). For each $u_i^j \in \mathbb{E}^j$, $i = 0 \dots f$, there is one

Kasner fixed point in each sector given by $\check{u}_i^j(u_i^j)$ in Table 1, which thereby leads to $6\lfloor u_0^j \rfloor$ fixed points on K° for the j^{th} Kasner era, denoted by $\check{\mathbb{E}}^j$.

As follows from the above, a change of Kasner epochs without a change of Kasner eras with $u_k^j \in (2, \infty)$ yields a piece of a heteroclinic network corresponding to $\overline{\mathcal{T}}_{R_1 N_-}(\check{u}_k^j = 1/u_k^j)$, where $\check{u}_k^j \in (132)_c$, see Figure 10 (left), while a change of the j^{th} era to the $(j+1)^{\text{th}}$ era corresponds to $\overline{\mathcal{T}}_{R_1 N_-}(\check{u}_f^j = 1/u_f^j)$ where $\check{u}_f^j \in (\frac{1}{2}, 1) = (132)_f$, see Figure 10 (right). Hence, the full heteroclinic network associated with the j^{th} era of length $\lfloor u_0^j \rfloor$ is obtained by taking the following union:

$$(63) \quad \mathbb{H}^j := \left(\bigcup_{\check{u} \in \check{\mathbb{E}}^j \cap (321)} \overline{\mathcal{T}}_{R_1 R_3}(\check{u}) \right) \cup \left(\bigcup_{\check{u} \in \check{\mathbb{E}}^j \cap (132)} \overline{\mathcal{T}}_{R_1 N_-}(\check{u}) \right),$$

where $\overline{\mathcal{T}}_{R_1 R_3}(\check{u})$ and $\overline{\mathcal{T}}_{R_1 N_-}(\check{u})$ denote the closure of the respective double frame and mixed curvature-frame transitions.

Since all heteroclinic orbits arising from points $\check{u} \in \check{\mathbb{E}}^j \setminus [(321) \cup (132)]$ are contained in one of the closures above, the *single transition network* of the j^{th} era is given by the heteroclinic chains that form the boundaries of the era network (63), i.e.,

$$(64) \quad \partial\mathbb{H}^j := \left(\bigcup_{\check{u} \in \check{\mathbb{E}}^j \cap (321)} \partial\overline{\mathcal{T}}_{R_1 R_3}(\check{u}) \right) \cup \left(\bigcup_{\check{u} \in \check{\mathbb{E}}^j \cap (132)} \partial\overline{\mathcal{T}}_{R_1 N_-}(\check{u}) \right).$$

Finally, the entire heteroclinic network associated with a frame-invariant Kasner sequence $\{u_0, u_1, u_2, \dots\}$ is obtained by taking the union of the heteroclinic networks, i.e., $\cup_j \mathbb{H}^j$, while the heteroclinic network of single transitions is given by $\cup_j \partial\mathbb{H}^j$.

Thus, in the hexagon representation there are two main steps to construct general heteroclinic chains corresponding to a frame-invariant Kasner sequence $\{u_0, u_1, u_2, \dots\}$, which in turn is partitioned into a sequence of eras according to (62). First, we identify the hexagons corresponding to each value of u in the Kasner sequence and then divide them according to the different eras they belong to. Second, we connect the different hexagons with the BKL map rules depicted in Figure 10, where the rule for era continuation (Figure 10 (left)) yields a representation for the era network in (63), while the rule for era change (Figure 10 (right)) enables us to take the union of two different era networks. This allows us to obtain a representation for the entire heteroclinic network $\cup_j \mathbb{H}^j$ corresponding to the Kasner sequence $\{u_0, u_1, u_2, \dots\}$.

The golden ratio for which $u_0 = u_f = (1 + \sqrt{5})/2$, discussed in the next section, is the only Kasner sequence with $u_0^{j+1} = u_f^j$ for all $j = 0, 1, 2, \dots$; all other frame-invariant Kasner sequences involve eras where $u_0^{j+1} \neq u_f^j$ for some j . Such Kasner sequences yield *isolated fixed points* from which *isolated heteroclinic orbits* originate, which gives rise to *isolated heteroclinic chains*, where the notation isolated stands for that these structures are not connected to preceding non-isolated heteroclinic chains in the heteroclinic network corresponding to such Kasner sequences. To illustrate these features by means of the hexagon-graph representation, we will consider an example, given in Figure 11, corresponding to a Kasner sequence characterized by a continued fraction given by $u_0 = [2; 4, 2, 1, 2, 1, 2, 2, 2, \dots]$. Note that this example also includes the ingredients

for obtaining the cyclic heteroclinic networks and their properties for the periodic Kasner sequences in the following section.²³

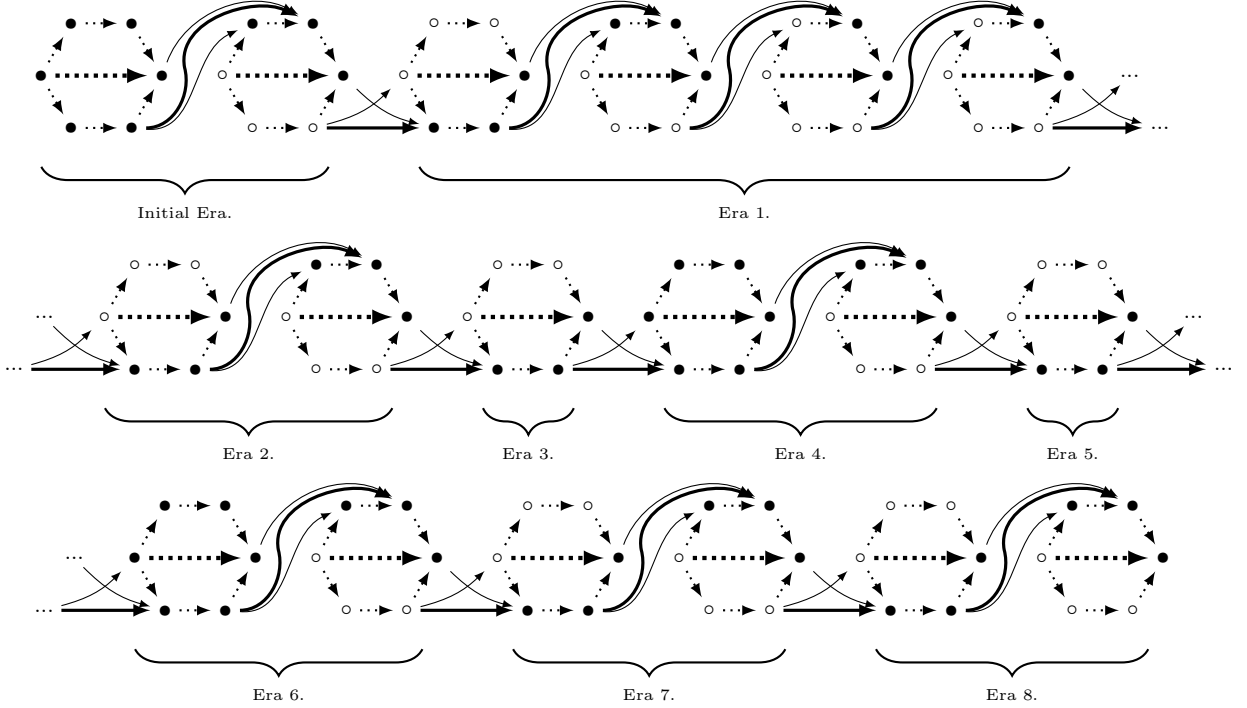


Figure 11: An example of a subnetwork of heteroclinic chains. When an era has a length longer than one, this gives rise to isolated fixed points, denoted by hollow circles, from which isolated heteroclinic orbits and chains originate. These isolated structures are not connected to earlier non-isolated heteroclinic chains. Since the isolated structures cannot be shadowed by Bianchi type $VI_{-1/9}$ solutions that shadow preceding non-isolated heteroclinic chains, they are not expected to play an asymptotic role for such solutions. Hence, they should be removed to yield the relevant heteroclinic network.

The above example illustrates how one constructs general aperiodic (and periodic) heteroclinic chains, where the main ingredient is how to connect hexagons due to the BKL map being an era change or not. In particular, concatenations of such connections between hexagons describe the isolated pieces that should be removed. The identification of isolated fixed points, heteroclinic orbits and chains depends on the length of an era and if the preceding era has a length longer than one or not. This is illustrated in Figure 11, which yields the following general rules for identifying isolated structures:

- (r₁) If the j^{th} era has length $[u_0^j] = k_j = 1$, then the first hexagon in the subsequent $(j+1)^{\text{th}}$ era has no isolated fixed points, heteroclinic orbits and chains, as exemplified in Figure 11 in the transition from era 3 to 4 and era 5 to 6.
- (r₂) If the j^{th} era has length $[u_0^j] = k_j \geq 2$, then all hexagons within the j^{th} era, except the first (which corresponds to the largest value of the Kasner parameter in that era, i.e. u_0^j), contain an *isolated heteroclinic chain* $(321) \cdots \blacktriangleright (231) \cdots \blacktriangleright (132) \cdots \blacktriangleright (123)$, an *isolated heteroclinic orbit* $(321) \cdots \blacktriangleright (312)$, and *isolated double frame transition*

²³We expect that there are Bianchi type $VI_{-1/9}$ orbits that shadow heteroclinic chains in the heteroclinic network associated with a Kasner sequence. Note, however, that isolated heteroclinic fixed points, orbits and chains in the corresponding heteroclinic network cannot be shadowed by an orbit that has begun to shadow a heteroclinic chain in the network that precedes such isolated structures.

orbits $(321)\cdots\blacktriangleright(123)$, with no previous non-isolated heteroclinic orbit connections in the Kasner sequence heteroclinic network.

- (r₃) If the j^{th} era has length $\lfloor u_0^j \rfloor = k_j \geq 2$, then the mixed curvature-frame transition orbits $(132) \blacktriangleright (231)$ from the j^{th} to the $(j+1)^{\text{th}}$ era are isolated, as is the single curvature transition orbit $(132) \blacktriangleright (123)$ which is followed by the thereby isolated heteroclinic chain $(321)\cdots\blacktriangleright(312)\cdots\blacktriangleright(213)\cdots\blacktriangleright(123)$, the heteroclinic orbit $(321)\cdots\blacktriangleright(231)$, and the double frame transition orbits $(321)\cdots\blacktriangleright(123)$ in the first hexagon with u_0^{j+1} in the $(j+1)^{\text{th}}$ era, see era 0 to 1, era 1 to 2, era 2 to 3, era 4 to 5, era 6 to 7, and era 7 to 8 in Figure 11.
- (r₄) When the j^{th} era has length $\lfloor u_0^j \rfloor = k_j \geq 3$, in addition to the isolated structures given in (r₂) and (r₃), all hexagons within the j^{th} era, except the first (with u_0^j) and second (with u_1^j), prolong the isolated heteroclinic orbit $(321)\cdots\blacktriangleright(312)$ in (r₂) to the isolated heteroclinic chain $(321)\cdots\blacktriangleright(312)\cdots\blacktriangleright(213)$. Moreover, this also leads to that the single heteroclinic curvature transition $(132) \rightsquigarrow (312)$ and the mixed curvature-frame transition orbits $(132) \rightsquigarrow (213)$ that connect the hexagons after the first two Kasner epochs within the era become isolated, see era 1 in Figure 11.

We emphasize that the above discussion takes into account general infinite heteroclinic chains, regardless if they are aperiodic or periodic. The heteroclinic network corresponding to an aperiodic Kasner sequence is constructed according to the above guidelines while the network corresponding to a periodic Kasner sequence is obtained by considering an infinite sequence of hexagons with repeated copies of heteroclinic subnetworks, which amounts to appropriately identifying repeated objects, once a period is realized, in the quotient topology.

Lastly, we summarize the above in the following Proposition, which describes the construction of general heteroclinic chains that are expected to be shadowed by Bianchi type VI_{-1/9} solutions:

Proposition 3.3. *Consider an initial frame-invariant Kasner parameter $u_0 \in [1, \infty)$ with orbit under the BKL map (47) given by $\{u_0, u_1, \dots, u_k, \dots\}$, partitioned into eras according to (48). The following algorithm yields a construction of general heteroclinic chains:*

- (i) *Each u_k yields six values for the generalized Kasner parameter $\check{u}_n \in \mathbb{R}$ connected by heteroclinic orbits into the hexagon graph in Figure 9.*
- (ii) *Hexagons are connected by two possible configurations depending on if the BKL map (47) changes era or not, shown in Figure 10.*
- (iii) *Only a subset of the fixed points $\{\check{u}_1, \dots, \check{u}_n, \dots\}$ and their corresponding heteroclinic orbits that originate from them are non-isolated, i.e. the complement to the isolated structures described in (r₁), (r₂), (r₃) and (r₄).*

Finally, the work [21] introduced the concept of large and small curvature phases and generalized the stochastic analysis in [34], which shows that one is most likely to be in a Kasner epoch in a small curvature phase, which entails a large value of u . As follows from the removal rules (r₁) – (r₄) of isolated heteroclinic chains in Proposition 3.3 this implies that most multiple transitions are removed. In the present state space a small curvature phase corresponds to being mostly in a small neighborhood of the Taub point T₃, which leads to a sequence of alternating single frame transitions \mathcal{T}_{R_3} from sector (213) to sector

(123) and single curvature transitions \mathcal{T}_{N_-} from sector (123) to sector (213), as illustrated by Era 1 in Figure 11. Thus most of the multiple transitions are statistically expected to be removed. This however, is not the case for networks of entangled cyclic heteroclinic chains discussed next.

4. Examples of networks of cyclic heteroclinic chains

Repeated (finite) frame-invariant Kasner epoch sequences, and thereby also repeated era sequences, can be translated to heteroclinic cyclic networks by means of Proposition 3.3 and our graphical representation, which also enable removing the isolated heteroclinic chains from these cyclic networks and thereby obtain their stable parts. Next we will illustrate this by considering three examples:²⁴ the metallic ratios given by the golden and silver ratios with an era sequence with period one, $u_0 = \frac{1+\sqrt{5}}{2}$ and $u_0 = 1 + \sqrt{2}$, respectively, and one with an era sequence with period two, $u_0 = 1 + \sqrt{3}$.

4.1. The golden ratio $u_0 = \frac{1+\sqrt{5}}{2}$

The golden ratio $u_0 = [(1)] = (1 + \sqrt{5})/2$ leads to that both the frame-invariant Kasner sequence and the era sequence have period 1,

$$(65) \quad (u_i)_{i \in \mathbb{N}_0} : \quad \frac{1+\sqrt{5}}{2} \rightarrow \frac{1+\sqrt{5}}{2} \rightarrow \frac{1+\sqrt{5}}{2} \rightarrow \frac{1+\sqrt{5}}{2} \rightarrow \dots,$$

where the Kretschmann scalar in (17) for $u_0 = (1 + \sqrt{5})/2$ is given by $\mathcal{W}((1 + \sqrt{5})/2) = 27(5 - 2\sqrt{5})/8 \approx 1.781\dots$

As described in (r_1) , an era that follows an era of length one has no isolated fixed points, heteroclinic orbits and chains. Since the golden ratio consists of a sequence of eras with length one, there are thereby no isolated fixed points, heteroclinic orbits and chains in this case. It follows straightforwardly by applying the rules given in the previous section that the heteroclinic network, when expressed in the symbolic hexagon representation, takes the form given in Figure 12.

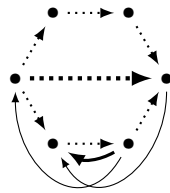


Figure 12: A graph that describes the possible itineraries of the heteroclinic network associated with $u_0 = (1+\sqrt{5})/2$. Thin dotted arrows depict single frame transitions whereas the bold dotted arrow describe double frame transitions; single curvature transitions are denoted by curved thin arrows while mixed curvature-frame transitions are depicted by a thick curved arrow. The leftmost point denotes $\tilde{u} = -(\sqrt{5} - 1)/2$ in sector (321) while the rightmost point corresponds to $\tilde{u} = u = (\sqrt{5} + 1)/2$ in sector (123).

²⁴Periodic cycles of period 13 and 18 have previously been found numerically in [8]

The graph representation in Figure 12 for the golden ratio, $u_0 = \frac{1+\sqrt{5}}{2}$, in combination with the projection rules onto the plane $\Sigma_1 + \Sigma_2 + \Sigma_3 = 0$ in $(\Sigma_1, \Sigma_2, \Sigma_3)$ -space described in Sections 2.2 (see Figure 3) and 2.3 (see Figure 4) for the various transitions, amounts to the following full heteroclinic network according to (63):

$$(66) \quad \mathbb{H}_{\text{Golden}} = \overline{\mathcal{T}}_{R_1 R_3}(\check{u} \in (321)) \cup \overline{\mathcal{T}}_{R_1 N_-}(\check{u} \in (132)).$$

This is illustrated in Figure 13, in addition to the network of single transitions described in (64), given by

$$(67) \quad \partial \mathbb{H}_{\text{Golden}} = \partial \overline{\mathcal{T}}_{R_1 R_3}(\check{u} \in (321)) \cup \partial \overline{\mathcal{T}}_{R_1 N_-}(\check{u} \in (132)),$$

where $\check{u} = -(\sqrt{5} - 1)/2 \in (321)$ and $\check{u} = (\sqrt{5} - 1)/2 \in (132)$.

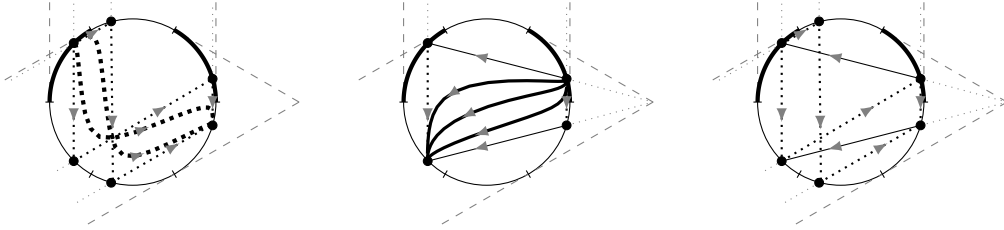


Figure 13: Projection onto the $\Sigma_1 + \Sigma_2 + \Sigma_3 = 0$ plane in $(\Sigma_1, \Sigma_2, \Sigma_3)$ -space of the heteroclinic network induced by the frame-invariant golden ratio Kasner parameter $u_0 = \frac{1+\sqrt{5}}{2}$. **Left:** The frame transition network $\overline{\mathcal{T}}_{R_1 R_3}(\check{u})$ for $\check{u} = -(\sqrt{5} - 1)/2 \in (321)$; single frame transitions are denoted by thin dotted directed lines while double frame transitions are illustrated by two representative solutions denoted by directed thick dotted lines. **Middle:** The curvature transition network $\overline{\mathcal{T}}_{R_1 N_-}(\check{u})$ for $\check{u} = (\sqrt{5} - 1)/2 \in (132)$; single curvature transitions are given by directed thin lines while mixed curvature-frame solutions are depicted as directed thicker lines. The full heteroclinic network of the golden ratio Kasner parameter is given by the union of the frame and curvature transition networks. **Right:** Depiction of the single transition network $\partial \overline{\mathcal{T}}_{R_1 R_3}(\check{u} \in (321)) \cup \partial \overline{\mathcal{T}}_{R_1 N_-}(\check{u} \in (132))$.

One of the uses of the hexagonal representation is that it easily identifies the different cyclic subnetworks, which we depict in the $\Sigma_1 + \Sigma_2 + \Sigma_3 = 0$ plane in the $(\Sigma_1, \Sigma_2, \Sigma_3)$ -space projected representation in Figure 14. Single transitions form heteroclinic cycles with period 3 and 6; double frame transitions yield heteroclinic cycles with period 4 (replacing the former period 6 chains); mixed curvature-frame transitions leads to heteroclinic cycles with period 2.

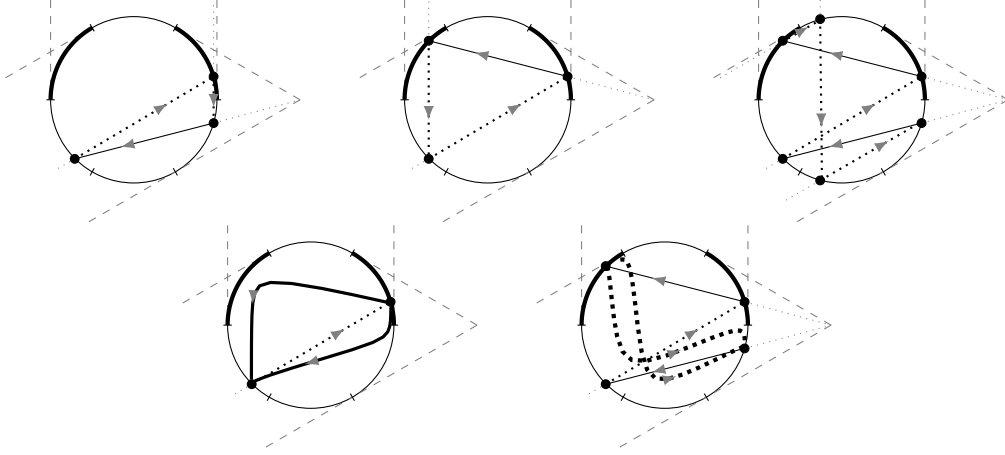


Figure 14: Cyclic subnetworks of heteroclinic chains associated with $u_0 = \frac{1+\sqrt{5}}{2}$ in Figure 13. **Top:** three chains with period 3 and 6 consisting of single transitions; these chains correspond to the cycles in Figure 12. **Bottom:** two one-parameter families of chains containing a double frame or mixed curvature-frame transition. Note that each of the bottom one-parameter families of heteroclinic chains possesses the two above adjacent single heteroclinic transition subnetworks as boundaries.

The heteroclinic chains that arise from the golden ratio $u_0 = \frac{1+\sqrt{5}}{2}$ are the simplest candidates to prove a stable manifold, akin to what was done in [2, 37, 38, 3]. However, the methods used in those works can not be directly applied to the present case. On the one hand, the methods in [37, 38, 3] require an appropriate ordering of the eigenvalues, which does not occur here, as shown in Table 3. In particular, since all possible heteroclinic chains arising from $u_0 = \frac{1+\sqrt{5}}{2}$ have a point in the multivalued region $\mathbf{A}_{R_1 N_-}^- = (321)$, a different local analysis is necessary for an eventual proof. On the other hand, it was shown in [8, Chapter 5] that the 3-cycle in Figure 14 (Top and Middle) associated with the golden ratio $u_0 = (1 + \sqrt{5})/2$ does not satisfy the Sternberg Non-Resonance Conditions, and thereby does not support a Takens linearization – a tool used for the proof of Béguin in [2].

\tilde{u}	Sector	λ_{R_1}	λ_{R_3}	λ_{N_-}	λ_A	Eigenvalues Order
$-\frac{(3+\sqrt{5})}{2}$	(213)	$-\frac{3\sqrt{5}}{2}$	$\frac{3(1+\sqrt{5})}{4}$	-3	$-\frac{3(3-\sqrt{5})}{4}$	$-\lambda_A < \lambda_{R_3} < -\lambda_{N_-} < -\lambda_{R_1}$
$-\frac{(1+\sqrt{5})}{2}$	(231)	$-\frac{3(1+\sqrt{5})}{4}$	$\frac{3\sqrt{5}}{2}$	$-\frac{3(1+\sqrt{5})}{2}$	$-\frac{3}{2}$	$-\lambda_A < -\lambda_{R_1} < \lambda_{R_3} < -\lambda_{N_-}$
$-\frac{(\sqrt{5}-1)}{2}$	(321)	$\frac{3(1+\sqrt{5})}{4}$	$\frac{3(\sqrt{5}-1)}{4}$	$-\frac{3(1+\sqrt{5})}{2}$	$-\frac{3(3+\sqrt{5})}{4}$	$\lambda_{R_3} < \lambda_{R_1} < -\lambda_A < -\lambda_{N_-}$
$-\frac{(3-\sqrt{5})}{2}$	(312)	$\frac{3\sqrt{5}}{2}$	$-\frac{3(\sqrt{5}-1)}{4}$	-3	$-\frac{3(3+\sqrt{5})}{4}$	$-\lambda_{R_3} < -\lambda_{N_-} < \lambda_{R_1} < -\lambda_A$
$\frac{(\sqrt{5}-1)}{2}$	(132)	$\frac{3(\sqrt{5}-1)}{4}$	$-\frac{3\sqrt{5}}{2}$	$\frac{3(\sqrt{5}-1)}{2}$	$-\frac{3}{2}$	$\lambda_{R_1} < -\lambda_A < \lambda_{N_-} < -\lambda_{R_3}$
$\frac{(1+\sqrt{5})}{2}$	(123)	$-\frac{3(\sqrt{5}-1)}{4}$	$-\frac{3(1+\sqrt{5})}{4}$	$\frac{3(\sqrt{5}-1)}{2}$	$-\frac{3(3-\sqrt{5})}{4}$	$-\lambda_A < -\lambda_{R_1} < \lambda_{N_-} < -\lambda_{R_3}$

Table 3: The \tilde{u} parametrization of each fixed point of the heteroclinic network corresponding to the golden ratio $u = \frac{1+\sqrt{5}}{2}$ in the 6 different sectors, ordered by increasing \tilde{u} parameter, and the corresponding eigenvalues and their ordering.

4.2. The silver ratio $u_0 = 1 + \sqrt{2}$

The silver ratio $u_0 = [(2)] = 1 + \sqrt{2}$ yields an era sequence of period 1, but a frame-invariant Kasner sequence with period 2:

$$(68) \quad (u_i)_{i \in \mathbb{N}_0} : \underbrace{(1 + \sqrt{2}) \rightarrow \sqrt{2}}_{\text{era}} \rightarrow \underbrace{(1 + \sqrt{2}) \rightarrow \sqrt{2}}_{\text{era}} \rightarrow \underbrace{(1 + \sqrt{2}) \rightarrow \sqrt{2}}_{\text{era}} \rightarrow \dots,$$

for which the Kretschmann scalar in (17) is given by $\mathcal{W}(1 + \sqrt{2}) = 54(44 - 25\sqrt{2})/343 \approx 1.360\dots$ and $\mathcal{W}(\sqrt{2}) = 162/(3 + \sqrt{2})^3 \approx 1.883\dots$

Each of the two frame-invariant Kasner parameter values, $u \in \{1 + \sqrt{2}$ and $\sqrt{2}\}$, yields six values of \tilde{u} , one in each sector, resulting in a pair of fixed points in each sector and a total of twelve points on the Kasner circle K° , described in Table 4:

u	\tilde{u}	Sector
$\sqrt{2}$ $1 + \sqrt{2}$	$-(\sqrt{2} + 1)$ $-(\sqrt{2} + 2)$	(213)
$1 + \sqrt{2}$ $\sqrt{2}$	$-\sqrt{2}$ $-(\frac{1}{\sqrt{2}} + 1)$	(231)
$\sqrt{2}$ $1 + \sqrt{2}$	$-(2 - \sqrt{2})$ $-\frac{1}{\sqrt{2}}$	(321)
$1 + \sqrt{2}$ $\sqrt{2}$	$-(1 - \frac{1}{\sqrt{2}})$ $-(\sqrt{2} - 1)$	(312)
$\sqrt{2}$ $1 + \sqrt{2}$	$\frac{1}{\sqrt{2}}$ $\sqrt{2} - 1$	(132)
$1 + \sqrt{2}$ $\sqrt{2}$	$1 + \sqrt{2}$ $\sqrt{2}$	(123)

Table 4: The parametrization by u and \tilde{u} for each fixed point in the various sectors on the Kasner circle K° of the heteroclinic network corresponding to the silver ratio $u_0 = 1 + \sqrt{2}$. The Kasner fixed points associated with $1 + \sqrt{2}$ and $\sqrt{2}$ are denoted by black and lightgray dots, respectively. The table is organized by increasing \tilde{u} .

Applying the methods of Sections 2.2 and 2.3, we obtain Figure 15, which depicts the corresponding hexagonal representation of the heteroclinic network. This follows from the last two eras of length 2 in the example in Figure 11, including the isolated fixed points, heteroclinic orbits and chains.

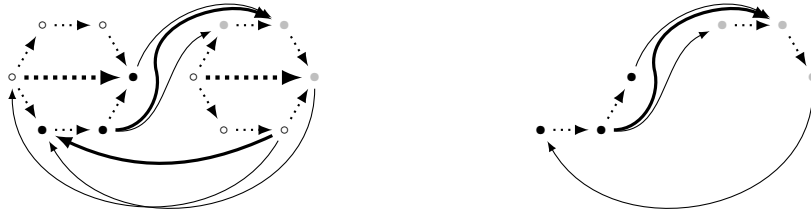


Figure 15: Left: The hexagonal graph representation describing the heteroclinic network of the periodic Kasner sequence induced by the silver ratio $u_0 = 1 + \sqrt{2}$ (hexagon with black dots) and its iterate $u = \sqrt{2}$ (hexagon with lightgray dots). **Right:** The relevant network for the asymptotic dynamics, obtained by removing the isolated parts of the heteroclinic network. This yields three distinct heteroclinic cycles, described in Figure 17.

Using the values for \check{u} in sectors (321) and (132) in Table 4 for $u = 1 + \sqrt{2}$ and $\sqrt{2}$ leads to the general construction of the heteroclinic network (63) that takes the form

$$(69) \quad \mathbb{H}_{\text{Silver}} = \overline{\mathcal{T}}_{R_1 R_3} \left(\check{u} = -\frac{1}{\sqrt{2}} \right) \cup \overline{\mathcal{T}}_{R_1 R_3} \left(\check{u} = -(2 - \sqrt{2}) \right) \\ \cup \overline{\mathcal{T}}_{R_1 N_-} \left(\check{u} = \sqrt{2} - 1 \right) \cup \overline{\mathcal{T}}_{R_1 N_-} \left(\check{u} = \frac{1}{\sqrt{2}} \right),$$

while the single transitions result in

$$(70) \quad \partial \mathbb{H}_{\text{Silver}} = \partial \overline{\mathcal{T}}_{R_1 R_3} \left(\check{u} = -\frac{1}{\sqrt{2}} \right) \cup \partial \overline{\mathcal{T}}_{R_1 R_3} \left(\check{u} = -(2 - \sqrt{2}) \right) \\ \cup \partial \overline{\mathcal{T}}_{R_1 N_-} \left(\check{u} = \sqrt{2} - 1 \right) \cup \partial \overline{\mathcal{T}}_{R_1 N_-} \left(\check{u} = \frac{1}{\sqrt{2}} \right).$$

Using the projection rules onto the plane $\Sigma_1 + \Sigma_2 + \Sigma_3 = 0$ in $(\Sigma_1, \Sigma_2, \Sigma_3)$ -space in sections 2.2 (see Figure 3) and 2.3 (see Figure 4) for the above various transitions yields the depiction in Figure 16.

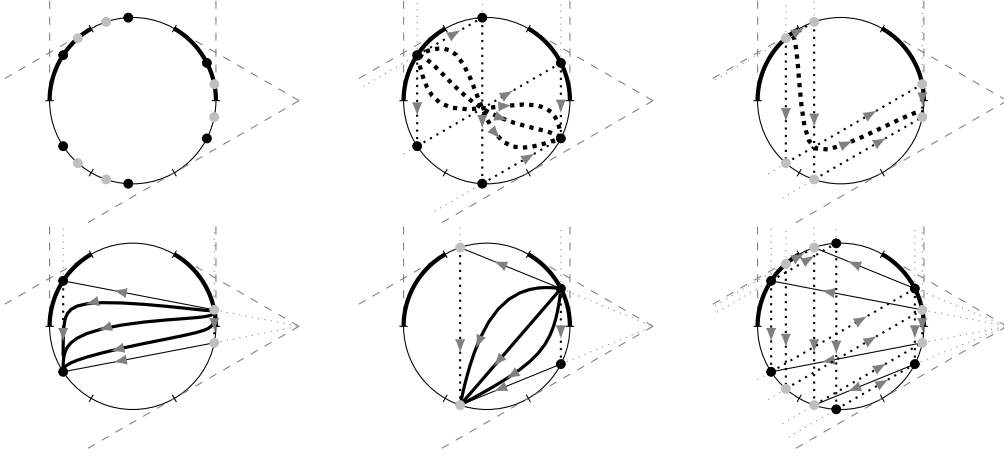


Figure 16: The Kasner fixed points associated with $1 + \sqrt{2}$ and $\sqrt{2}$ in black and lightgray dots, respectively, and representations of the heteroclinic networks of the closure of the various double frame and mixed curvature-frame transitions (the two upper right and lower left figures) induced by the silver ratio $u_0 = 1 + \sqrt{2}$. The entire heteroclinic network is obtained by taking the union of these closures, i.e., by superimposing the various network figures, while the single transition network (lower figure to the right) is obtained by superimposing their single transition boundaries. There are thereby 4 one-parameter families of multiple transitions containing a total of 16 single transitions on their boundaries.

If there are solutions that are attracted to the entangled cyclic heteroclinic network induced by the silver ratio $u_0 = 1 + \sqrt{2}$, then they cannot asymptotically shadow the isolated heteroclinic structure. For this reason we remove this structure in Figure 15 to the right. Combining the information in this figure with Figure 16 yields Figure 17, which contains two heteroclinic boundary chains consisting of single transitions which yield period 5 cycles, whereas the mixed curvature-frame transitions $\mathcal{T}_{R_1 N_-}$ result in heteroclinic chains with period 4 (replacing single transitions in the former period 5 chains).

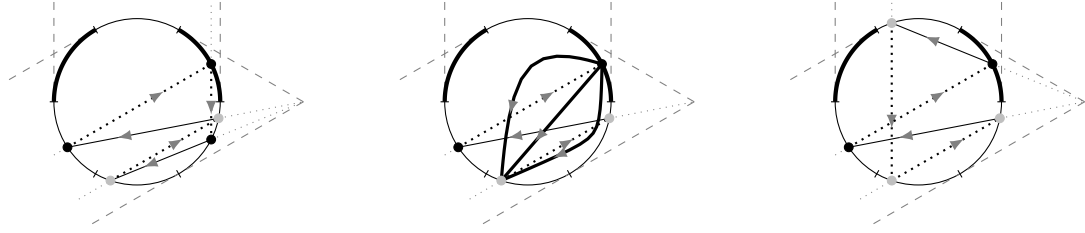


Figure 17: The stable subnetwork of cyclic heteroclinic chains associated with the silver ratio $u_0 = 1 + \sqrt{2}$, obtained from Figures 15 and 16. It consist of two cyclic period 5 heteroclinic single transition chains (left and right), and cyclic period 4 heteroclinic chains involving a mixed curvature-frame transition (middle).

The dynamical importance of the heteroclinic network arising from $u = 1 + \sqrt{2}$ is due to that the eigenvalues in sector (132) associated with the instability of R_1 and N_- , given by (19a) and (19c), respectively, are equal. This follows from that $\lambda_{R_1} = 3(1 - \tilde{u}^2)/f(\tilde{u})$ and $\lambda_{N_-} = 6\tilde{u}/f(\tilde{u})$, where $\tilde{u} = \sqrt{2} - 1$ (see Table 4) yields $\lambda_{R_1} = \lambda_{N_-}$, while $\lambda_{R_1} > \lambda_{N_-}$ when $\tilde{u} \in (0, \sqrt{2} - 1)$ and $\lambda_{N_-} > \lambda_{R_1}$ when $\tilde{u} \in (\sqrt{2} - 1, 1)$. Note that when $\lambda_{R_1} = \lambda_{N_-}$ for $\tilde{u} = \sqrt{2} - 1$ there exists a special orbit that is a straight line given by $\Sigma_1 = -2(1 - \Sigma_3)$ in $(\Sigma_1, \Sigma_2, \Sigma_3)$ -space, as shown in Appendix A.3. Due to this, these chains may play a role in a possible construction of a stable manifolds, akin to that in [2, 37, 38, 3].

4.3. The alloy ratio $u_0 = 1 + \sqrt{3}$

The alloy ratio²⁵ $u_0 = [2; (1, 2)] = 1 + \sqrt{3}$ yields an era sequence of period 2 and a frame-invariant Kasner sequence with period 3:

$$(71) \quad (u_i)_{i \in \mathbb{N}} : \underbrace{1 + \sqrt{3} \rightarrow \sqrt{3}}_{\text{era}} \rightarrow \underbrace{\frac{1+\sqrt{3}}{2}}_{\text{era}} \rightarrow \underbrace{1 + \sqrt{3} \rightarrow \sqrt{3}}_{\text{era}} \rightarrow \underbrace{\frac{1+\sqrt{3}}{2}}_{\text{era}} \rightarrow \dots,$$

for which the Kretschmann scalar in (17) is given by $\mathcal{W}(1 + \sqrt{3}) = 22 - 12\sqrt{3} \approx 1.215 \dots$, $\mathcal{W}(\sqrt{3}) = 324/(4 + \sqrt{3})^3 \approx 1.720 \dots$ and $\mathcal{W}((1 + \sqrt{3})/2) = 54(223 - 84\sqrt{3})/2197 \approx 1.905 \dots$

The case $u = 1 + \sqrt{3}$ gives rise to two periodic eras and a periodic Kasner sequence with three values of $u \in \{1 + \sqrt{3}, \sqrt{3}, \frac{1+\sqrt{3}}{2}\}$ such that each value yields six fixed point on the Kasner circle K° , one in each sector, resulting in the values of \tilde{u} given in Table 5.

²⁵The continued fraction expansions given by $[(n)]$ for $n \in \mathbb{N}$ are called the *metallic ratios* (e.g. the golden, silver and bronze ratios occur respectively for $n = 1, 2, 3$). We therefore introduce this new nomenclature for the impure ratio $u_0 = [2; (1, 2)] = 1 + \sqrt{3}$.

u	\check{u}	Sector
$\frac{1+\sqrt{3}}{2}$ $\sqrt{3}$ $1 + \sqrt{3}$	$-\frac{3+\sqrt{3}}{2}$ $-(1 + \sqrt{3})$ $-(2 + \sqrt{3})$	(213)
$1 + \sqrt{3}$ $\sqrt{3}$ $\frac{1+\sqrt{3}}{2}$	$-\frac{1+\sqrt{3}}{2}$ $-(1 + \frac{1}{\sqrt{3}})$ $-\sqrt{3}$	(231)
$\frac{1+\sqrt{3}}{2}$ $\sqrt{3}$ $1 + \sqrt{3}$	$-\frac{1}{\sqrt{3}}$ $-\frac{3-\sqrt{3}}{2}$ $-(\sqrt{3} - 1)$	(321)
$1 + \sqrt{3}$ $\sqrt{3}$ $\frac{1+\sqrt{3}}{2}$	$-(2 - \sqrt{3})$ $-\frac{\sqrt{3}-1}{2}$ $-(1 - \frac{1}{\sqrt{3}})$	(312)
$\frac{1+\sqrt{3}}{2}$ $\sqrt{3}$ $1 + \sqrt{3}$	$\sqrt{3} - 1$ $\frac{1}{\sqrt{3}}$ $\frac{\sqrt{3}-1}{2}$	(132)
$1 + \sqrt{3}$ $\sqrt{3}$ $\frac{1+\sqrt{3}}{2}$	$1 + \sqrt{3}$ $\sqrt{3}$ $\frac{1+\sqrt{3}}{2}$	(123)

Table 5: The values of u and \check{u} for the Kasner sequence induced by $u = 1 + \sqrt{3}$. The table is organized by increasing \check{u} . We respectively denote the points associated with $1 + \sqrt{3}, \sqrt{3}, \frac{1+\sqrt{3}}{2}$ by black, gray and lightgray.

The hexagonal representation of the heteroclinic network follows straightforwardly from the example given in Figure 15 by considering eras 2 to 5, which results in Figure 18.

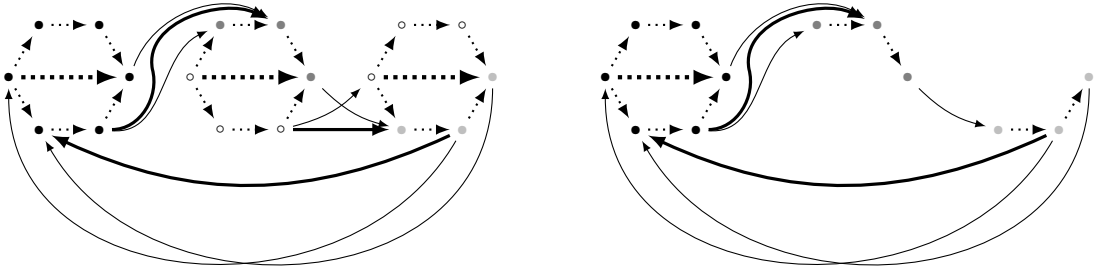


Figure 18: Left: Hexagonal graph representation describing the entangled cyclic heteroclinic network of the periodic Kasner sequence generated by $u = 1 + \sqrt{3}$. **Right:** Depiction of the network after removal of the isolated heteroclinic structure, which yields the remaining entangled cyclic heteroclinic network.

The entire cyclic heteroclinic network is obtained by taking the union $\mathbb{H}^0 \cup \mathbb{H}^1$ of the initial and the subsequent (first) era, where the relevant values for \check{u} for sectors (321) and (132) are to be inserted into equation (63) to yield the entire cyclic heteroclinic network, while equation (64) results in the single transition network, where the different transition elements are depicted in Figure 19.

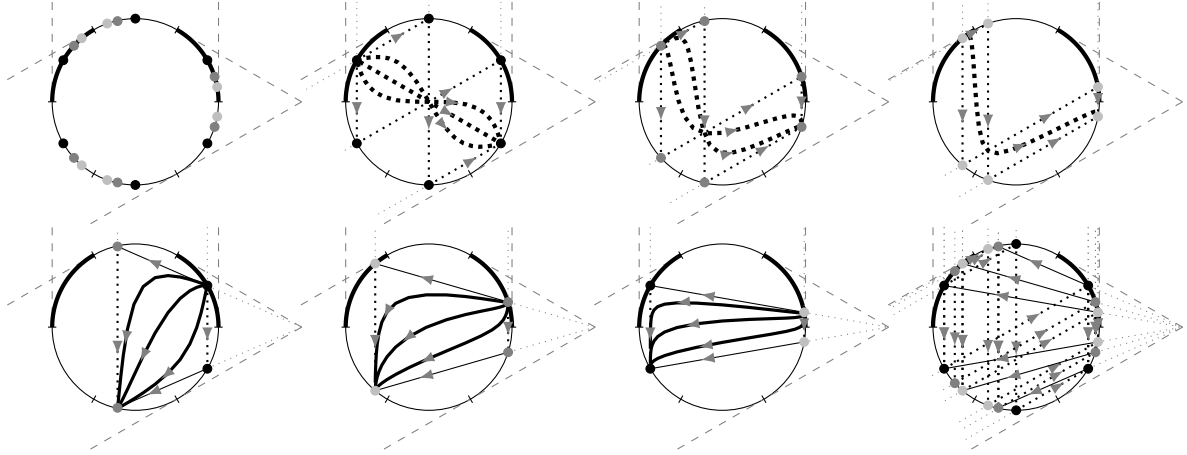


Figure 19: The 18 Kasner points associated with $u_0 = 1 + \sqrt{3}$, containing 3 points in each sector. In addition, the 6 one-parameter families of multiple transitions, whose boundaries yield the 24 single transitions.

The dynamical importance of the heteroclinic network arising from $1 + \sqrt{3}$ is due to the eigenvalues in sector (321) that are associated with the instability of R_1 and R_3 , respectively. These are given by $\lambda_{R_1} = 3(1 - \check{u}_0^2)/f(\check{u}_0)$ and $\lambda_{R_3} = -3(1 + 2\check{u}_0)/f(\check{u}_0)$ according to (19a) and (19b), which for the value $\check{u}_0 = 1 - \sqrt{3}$ leads to $\lambda_{R_1} = \lambda_{R_3}$, while $\lambda_{R_3} > \lambda_{R_1}$ when $\check{u} \in (-1, 1 - \sqrt{3})$ and $\lambda_{R_1} > \lambda_{R_3}$ when $\check{u} \in (1 - \sqrt{3}, -\frac{1}{2})$; these eigenvalue features presumably play a role in a possible construction of a stable manifolds, akin to that in [2, 37, 38, 3]. Note that the value $\check{u}_0 = 1 - \sqrt{3}$, where $\lambda_{R_1} = \lambda_{R_3}$, corresponds to the Kasner fixed point from which the particular explicit orbit with $R_1 = R_3$ and $\Sigma_2 = 0$, $\Sigma_3 = -\Sigma_1$, discussed previously in connection with double frame transitions, originates.

We emphasize that this heteroclinic network contains two special orbits, which are in the boundary of the set \mathcal{HO} ; see Section 2.5. The two Kasner fixed points with $\Sigma_- = \pm 1$, denoted by K_{\pm}° , where K_+° resides in sector (312) and has the following extended Kasner parameter value $\check{u} = -2 + \sqrt{3}$, while K_-° is in sector (213) with $\check{u} = -2 - \sqrt{3}$. Both these Kasner points correspond to the frame-invariant Kasner parameter $u = 1 + \sqrt{3}$, which notably characterizes the double frame transition for which $\lambda_{R_1} = \lambda_{R_3}$, discussed above.

The non-isolated heteroclinic network, shown in the right graph in Figure 18, contains five single transition heteroclinic cycles with period 8, which form the boundaries of one-parameter families of subnetworks containing either double-frame transitions $\mathcal{T}_{R_1 R_3}$ or mixed curvature-frame transitions $\mathcal{T}_{R_1 N_-}$, with a smaller period. The five single transition heteroclinic period 8 cycles are depicted in the $\Sigma_1 + \Sigma_2 + \Sigma_3 = 0$ plane in the $(\Sigma_1, \Sigma_2, \Sigma_3)$ -space representation in Figure 20.

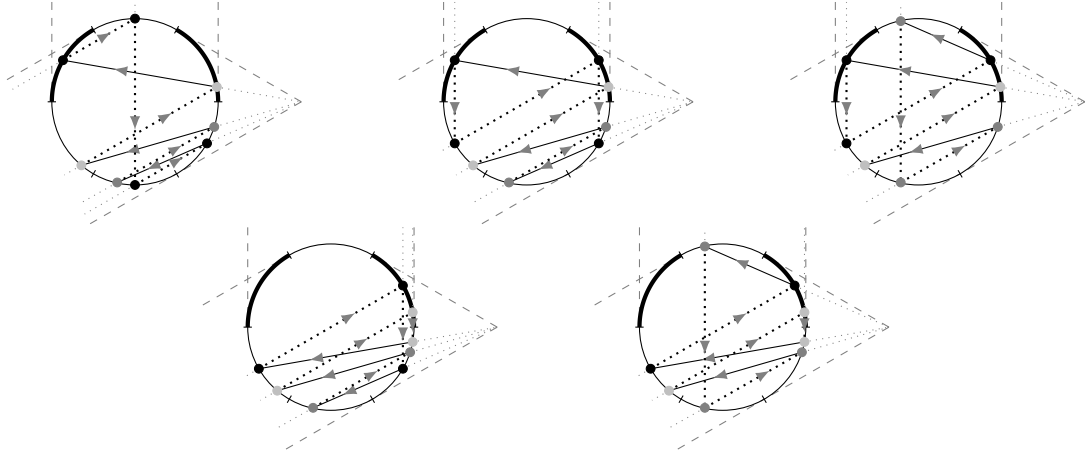


Figure 20: The five heteroclinic single transition period 8 cycles associated with $u = 1 + \sqrt{3}$. In addition, there are six cyclic subnetworks containing one-parameter families of multiple transitions, which we refrain from plotting.

Finally, note that for a general orbit of period n in the Kasner parameter u there are $6n$ points in the Kasner circle given by the parameter $\tilde{u}(u)$, with n points in each of the 6 sectors. Moreover, there are $8n$ single transitions and $2n$ sets of multiple transitions. There are thereby 4 sectors with a single possibility for single transitions and 2 sectors with two possible single transitions, which yield a total of $8n$ single transitions; whereas n points in each of the 2 sectors with multiple transitions yield $2n$ families of multiple transitions.

4.4. Comparisons between networks of type $VI_{-1/9}$ and type VIII, IX

Several properties can be inferred from a continued fraction representation of the frame-invariant Kasner parameters. Since the frame-invariant BKL map is the same for Bianchi type $VI_{-1/9}$ as for Bianchi type VIII and IX, we obtain the same characterization for all these models. However, the same development in u results in that type $VI_{-1/9}$ has a different continued fractional representation for the parameter $\tilde{u} \in \mathbb{R}$ than Bianchi type VIII and IX. Moreover, all sectors of the Kasner circle have a similar symmetric role in terms of the Bianchi type II dynamics of Bianchi type VIII and IX, which always yield single curvature transitions. This is not the case for type $VI_{-1/9}$, since the frame transitions do not amount to any change in the frame-invariant Kasner parametrization. The only relevant map that contributes to frame-invariant Kasner changes are the Bianchi type II curvature transitions in the sectors $(123) \cup (132)$. In particular, sector (132) that describes the set $\mathbf{A}_{R_1 N_-}^-$ plays a distinguished role for the type $VI_{-1/9}$ dynamics.

Given a point p in any sector $(\alpha\beta\gamma)$, all single transition heteroclinic chains eventually result in a point in the region $\mathbf{A}_{R_1 N_-}^-$, i.e. sector (132) , which is reached by a preceding \mathcal{T}_{R_3} transition from sector (231) . Any point in sector (321) either reaches sector (231) with a \mathcal{T}_{R_1} transition or (312) with a \mathcal{T}_{R_3} transition; any point in sector (312) is mapped to sector (213) by a \mathcal{T}_{R_1} transition followed by a \mathcal{T}_{R_3} transition that takes it to sector (123) . Finally, any point in sector (123) eventually reach sector (231) after finitely many iterates of the type $(\mathcal{T}_{R_3} \circ \mathcal{T}_{N_-})^n$.²⁶

²⁶The dynamical analysis associated with the Kasner circle maps for the extended Kasner parameter \tilde{u}

The differences of the discrete Kasner circle dynamics between type VIII, IX and type $VI_{-1/9}$ is exemplified by the networks of cyclic heteroclinic chains, illustrated by the golden ratio $u_0 = (1 + \sqrt{5})/2$. The heteroclinic structure that arises from this ratio for type $VI_{-1/9}$ was described in Figures 12, 13 (right) and 14. This can be compared with the heteroclinic structures for the golden ratio for type VIII, IX given in Figure 21 (left). Similarly, the heteroclinic network corresponding to the silver ratio $u_0 = 1 + \sqrt{2}$ for type $VI_{-1/9}$, described in Figures 15, 16 (lower right) and 17, can be compared with the silver ratio for the type VIII, IX structures given in Figure 21 (right). Note that the graphic representation we have introduced for type $VI_{-1/9}$, which emphasized the role of frame transitions, is of little use for the type VIII and IX vacuum models, for the simple reason that they do not exhibit such structures.

The present examples of cyclic heteroclinic networks in Sections 4.1, 4.2 and 4.3 are the simplest candidates for stable manifold theorems for Bianchi type $VI_{-1/9}$ of the type given by Liebscher et al. [37, 38] for Bianchi type VIII and IX. There are, however, several issues that arise when trying to adapt such proofs to type $VI_{-1/9}$. First, one has to take the present Gauss and Codazzi constraints into account, as not all eigenvalues in Table 3 pertain to the physical state space. Second, some Kasner fixed points in the cyclic network involve two unstable modes, something that did not occur in type VIII and IX. Third, the eigenvalue ordering in Liebscher et al. [37, 38] is not satisfied.

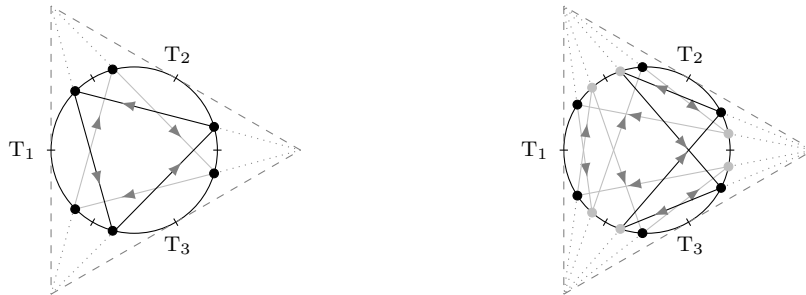


Figure 21: Left: Projection onto the $\Sigma_1 + \Sigma_2 + \Sigma_3 = 0$ plane in $(\Sigma_1, \Sigma_2, \Sigma_3)$ -space of the heteroclinic network induced by the frame-invariant golden ratio Kasner parameter $u_0 = \frac{1+\sqrt{5}}{2}$ for Bianchi type VIII and IX. The six points \tilde{u} possess the same six coordinates as in type $VI_{-1/9}$, as is also the case for the two \mathcal{T}_{N_-} single curvature transitions. Here, there are only two symmetric heteroclinic cycles (one in black and one in gray), in contrast to the three non-symmetric cycles (and two one-parameter families) for type $VI_{-1/9}$ in Figure 14. **Right:** Projection onto the $\Sigma_1 + \Sigma_2 + \Sigma_3 = 0$ plane in $(\Sigma_1, \Sigma_2, \Sigma_3)$ -space of the heteroclinic network induced by the frame-invariant silver ratio Kasner parameter $u_0 = 1 + \sqrt{2}$ for Bianchi type VIII and IX. The twelve points \tilde{u} possess the same twelve coordinates as those in type $VI_{-1/9}$, as is also the case for the four \mathcal{T}_{N_-} single curvature transitions. Here there are three symmetric heteroclinic cycles (one in black and two in gray), in contrast to the two non-symmetric cycles (and one one-parameter family) for type $VI_{-1/9}$ in Figure 17.

in Table 2 is not the same as the usual D_3 equivariant Kasner circle map in Bianchi type VIII and IX, since this symmetry is broken in Bianchi type $VI_{-1/9}$. However, to prove that the discrete type $VI_{-1/9}$ dynamics is chaotic one can presumably adapt the proof in [36] to the present setting.

A. Dynamics in invariant subsets

A.1. A toy model

In contrast to Bianchi type VIII and IX, the Bianchi type VI_{-1/9} models do not admit a Hamiltonian formulation, see e.g. [33] and references therein. However, in [21] a ‘dominant’ Hamiltonian was presented yielding a toy model that is expected to share the past asymptotic generic features with the present problem. This Hamiltonian can be written on the following form²⁷

$$(72) \quad H_{\text{Dom}} = \frac{1}{2} (-p_0^2 + p_+^2 + p_-^2) + \frac{1}{2} e^{2\sqrt{3}\beta^-} \left(A_1^2 e^{6\beta^+} + A_3^2 e^{-6\beta^+} \right) + \frac{1}{2} A_-^2 e^{4(\beta^0 + \beta^+ - \sqrt{3}\beta^-)} = 0,$$

where the future directed time variable t_T is called the Taub time. Introducing the variables

$$(73a) \quad \Sigma_+ = \frac{p_+}{-p_0}, \quad \Sigma_- = \frac{p_-}{-p_0},$$

$$(73b) \quad R_1 = \frac{A_1 e^{2\sqrt{3}\beta^- + 3\beta^+}}{-p_0}, \quad R_3 = \frac{A_3 e^{3\beta^+ - \sqrt{3}\beta^-}}{-p_0}, \quad N_- = \frac{A_- e^{2(\beta^0 + \beta^+ - \sqrt{3}\beta^-)}}{-p_0},$$

and the past directed time variable τ , defined by

$$(74) \quad \frac{d\tau}{dt_T} = -\frac{d\beta^0}{dt_T} = p_0,$$

leads to the following system of evolution equations (after having obtained the Hamiltonian equations from (72)) for the state vector $(\Sigma_+, \Sigma_-, R_1, R_3, N_-)$:

$$(75a) \quad \Sigma'_+ = 2(1 - \Sigma^2)\Sigma_+ - 3R_3^2 + 3R_1^2 + 2N_-^2,$$

$$(75b) \quad \Sigma'_- = 2(1 - \Sigma^2)\Sigma_- + \sqrt{3}(R_1^2 + R_3^2) - 2\sqrt{3}N_-^2,$$

$$(75c) \quad R'_1 = [2(1 - \Sigma^2) - 3\Sigma_+ - \sqrt{3}\Sigma_-]R_1,$$

$$(75d) \quad R'_3 = [2(1 - \Sigma^2) + 3\Sigma_+ - \sqrt{3}\Sigma_-]R_3,$$

$$(75e) \quad N'_- = -2(\Sigma^2 + \Sigma_+ - \sqrt{3}\Sigma_-)N_-,$$

and the constraint

$$(76) \quad 1 - \Sigma^2 - N_-^2 = 0,$$

where

$$(77) \quad \Sigma^2 = \Sigma_+^2 + \Sigma_-^2 + R_1^2 + R_3^2.$$

Replacing Σ_{\pm} with $\Sigma_1, \Sigma_2, \Sigma_3$ according to

$$(78) \quad \Sigma_1 = \Sigma_+ - \sqrt{3}\Sigma_-, \quad \Sigma_2 = -2\Sigma_+, \quad \Sigma_3 = \Sigma_+ + \sqrt{3}\Sigma_-,$$

²⁷Obtained by using the Misner parametrization $-b_1 = \beta^0 + \beta^+ - \sqrt{3}\beta^-$, $-b_2 = \beta^0 - 2\beta^+$, $-b_3 = \beta^0 + \beta^+ + \sqrt{3}\beta^-$ in [21], and hence $\Sigma_1 = \Sigma_+ - \sqrt{3}\Sigma_-$, $\Sigma_2 = -2\Sigma_+$, $\Sigma_3 = \Sigma_+ + \sqrt{3}\Sigma_-$.

results in the same equations as in (1) and (2) by setting $A = 0$ and ignoring the remaining constraint $N_- R_3 = 0$ after having set $A = 0$ in (2b).

To establish global results for this toy model we will use the methods in ch. 10 in [63] and in [25] to derive a monotonic function. As the first step we therefore make a boost transformation in the β^- direction in the projected diagonal minisuperspace characterized by the metric $\eta_{AB} = \text{diag}[-1, 1, 1]$ of the kinetic part of the Hamiltonian (whose form thereby is preserved), i.e.,

$$(79) \quad \bar{\beta}^0 = \gamma(\beta^0 - v\beta^-) \quad \text{and} \quad \bar{\beta}^- = \gamma(-v\beta^0 + \beta^-).$$

Next, we set

$$(80) \quad v = 2/(3\sqrt{3}) \quad \text{and} \quad \gamma = \frac{1}{\sqrt{1-v^2}} = \sqrt{\frac{27}{23}},$$

in order for the potential to explicitly exhibit a conformal exponential factor with a timelike variable with respect to the minisuperspace metric η_{AB} . The Hamiltonian now takes the form:

$$(81) \quad H_{\text{Dom}} = \frac{1}{2} (-\bar{p}_0^2 + \bar{p}_+^2 + \bar{p}_-^2) + \frac{1}{2} e^{\frac{4\sqrt{3}}{23}\bar{\beta}^0} \left(e^{\frac{18}{\sqrt{23}}\bar{\beta}^-} \left(A_1^2 e^{6\bar{\beta}^+} + A_3^2 e^{-6\bar{\beta}^+} \right) + A_-^2 e^{4\bar{\beta}^+ - \frac{28}{\sqrt{23}}\bar{\beta}^-} \right) = 0,$$

Finally, we exploit the results in ch. 10 in [63] and in [25] to use the above form of the potential to derive the following monotonic function

$$(82) \quad \Delta := \frac{(1 - v\Sigma_-)^2}{(R_1^4 R_3^{10} N_-^9)^{\frac{2}{23}}},$$

which evolves according to

$$(83) \quad \Delta' = \frac{4}{69} \left(\frac{27(\Sigma_- - v)^2 + 23\Sigma_+^2}{1 - v\Sigma_-} \right) \Delta,$$

where we recall that $v = 2/(3\sqrt{3})$. Hence Δ is monotonically growing, except at the fixed point (which is analogous to the RT fixed point in type VI_{-1/9}):

$$(84) \quad (\Sigma_+, \Sigma_-) = (0, v), \quad (R_1, R_3, N_-) = \frac{1}{3\sqrt{3}} (2, \sqrt{10}, 3),$$

where Δ takes its minimum value, which happens asymptotically when $\tau \rightarrow -\infty$, while $\Delta \rightarrow \infty$ when $\tau \rightarrow +\infty$ toward the initial singularity.

This implies that

$$(85) \quad \lim_{\tau \rightarrow +\infty} R_1 R_3 N_- = 0,$$

i.e., the future attractor in τ of the 4-dimensional state space resides on the union of the three 3-dimensional invariant subsets, where either $R_1 = 0$, $R_3 = 0$, or $N_- = 0$.

Presumably, an eventual proof of the analogue to the Conjecture 3.2 for equations (75) is simpler. In particular, one would need to show that the cross-terms $R_1 N_-$, $R_3 N_-$, $R_1 R_3$

go to zero toward the singularity. These cross-terms evolve according to the following equations:

$$(86a) \quad (R_1 R_3)' = -4 \left[\Sigma_+^2 + (\Sigma_- + \sqrt{3}/4)^2 + R_1^2 + R_3^2 - \frac{19}{16} \right] R_1 R_3,$$

$$(86b) \quad (R_1 N_-)' = -4 \left[(\Sigma_+ + 5/8)^2 + (\Sigma_- - \sqrt{3}/8)^2 + R_1^2 + R_3^2 - \frac{15}{16} \right] R_1 N_-,$$

$$(86c) \quad (R_3 N_-)' = -4 \left[(\Sigma_+ - 1/8)^2 + (\Sigma_- - \sqrt{3}/8)^2 + R_1^2 + R_3^2 - \frac{9}{16} \right] R_3 N_-.$$

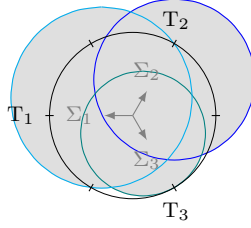


Figure 22: The shaded regions are the projection onto the plane $\Sigma_1 + \Sigma_2 + \Sigma_3 = 0$ in $(\Sigma_1, \Sigma_2, \Sigma_3)$ -space of the regions where each cross-term $R_1 N_-$ (blue), $R_3 N_-$ (teal) and $R_1 R_3$ (cyan) increases. Note that the (teal) ball is tangential to the Taub point T_3 , whereas the (cyan) ball crosses the Kasner circle at T_2 and Q_2 .

The evolution equations for the cross-terms according to the original system (1) are given by a perturbation of (86), since equations (86a), (86b) and (86c) have the extra terms, $-4R_1 N_- A$, $+3R_1 R_3 A$ and $(3R_3^2 - 4N_-^2)A$, respectively, where A is expected to be small toward the singularity. This suggests that the evolution of the cross-terms of the original system is similar to that of the cross-terms of the toy model when A is sufficiently small. This exemplifies the close relationship between the Bianchi type VI $_{-1/9}$ vacuum model and the toy model, which furthermore implies that if one cannot prove results for the simpler latter one then one is not likely to be able to prove results for the former.

We finally note that the Kasner and Bianchi type II invariant subsets of (75) coincide with the corresponding invariant sets of (1). Next we consider these subsets as well as the \mathcal{HO} subset of (1), where the latter, as we will see, is also related to the present Hamiltonian formulation.

A.2. The Kasner subset \mathcal{K}

Setting $A_- = 0$ (and hence $N_- = 0$) in the dominant Hamiltonian (72) leads to

$$(87) \quad H_{\mathcal{K}} = \frac{1}{2} (-p_0^2 + p_+^2 + p_-^2) + \frac{1}{2} e^{2\sqrt{3}\beta^-} \left(A_1^2 e^{6\beta^+} + A_3^2 e^{-6\beta^+} \right) = 0,$$

which is a Hamiltonian that correctly describes the Kasner subset \mathcal{K} . By setting $B^2 = |A_1 A_3|$, $C = \ln(|A_1/A_3|)$, this Hamiltonian can be written as

$$(88) \quad H_{\mathcal{K}} = \frac{1}{2} (-p_0^2 + p_+^2 + p_-^2) + B^2 e^{2\sqrt{3}\beta^-} \cosh(6\beta^+ + \alpha) = 0,$$

Since β^0 is a cyclic variable, it follows that the conjugate momentum p_0 is conserved, which leads to the reduced Hamiltonian

$$(89) \quad H_{\text{red}} = \frac{1}{2} (p_+^2 + p_-^2) + B^2 e^{2\sqrt{3}\beta^-} \cosh(6\beta^+ + C) = \frac{1}{2} p_0^2 = E = \text{constant}.$$

We note that since $\cosh(\cdot)$ is a symmetric function it follows that there exists a discrete symmetry, which in the dynamical system (1), with $A = 0 = N_-$, i.e. the Kasner subset \mathcal{K} , corresponds to invariance under interchanging 1 and 3 and making the transformation $(\Sigma_1, \Sigma_2, \Sigma_3) = -(\Sigma_1, \Sigma_2, \Sigma_3)$ (or letting $\tau \rightarrow -\tau$). Moreover, there exists a special solution corresponding to the minimum of $\cosh(6\beta^+ + C)$, i.e., at $6\beta^+ = -C = -\ln(|A_1/A_3|)$ with $p_+ = 0$. This leads to that $\Sigma_+ = 0$ with the present Misner parametrization, which corresponds to that $\Sigma_2 = 0$ and hence $\Sigma_1 = -\Sigma_3$, while $R_1 = R_3 > 0$, as also follows from the equations obtained by specializing (1) to the Kasner subset \mathcal{K} .

The above Hamiltonian problem is not obviously solvable. However, as pointed out in [40], the solutions, which correspond to double frame transitions, can be obtained from the original Kasner solution in a diagonal and Fermi-propagated frame by means of a coordinate transformation. We here present the solution for Σ_α , R_1 and R_3 in the time variable τ used in the main text in a simple and transparent form:²⁸

$$(90a) \quad \Sigma_1 = -1 + 3 \left[\frac{p_1 n_{20}^2 e^{-6p_1\tau} + p_2 n_{30}^2 e^{-6p_2\tau} + p_3 e^{-6p_3\tau}}{n_{20}^2 e^{-6p_1\tau} + n_{30}^2 e^{-6p_2\tau} + e^{-6p_3\tau}} \right],$$

$$(90b) \quad \Sigma_3 = -1 + 3 \left[\frac{p_1 e^{6p_1\tau} + p_2 n_{10}^2 e^{6p_2\tau} + p_3 (n_{10}n_{30} - n_{20})^2 e^{6p_3\tau}}{e^{6p_1\tau} + n_{10}^2 e^{6p_2\tau} + (n_{10}n_{30} - n_{20})^2 e^{6p_3\tau}} \right],$$

$$(90c) \quad R_1 = \frac{1}{\sqrt{3}} e^{-3\tau} \left[\frac{(3p_2 - 1 - \Sigma_3) n_{10} e^{6p_2\tau} + (3p_3 - 1 - \Sigma_3) n_{30} (n_{10}n_{30} - n_{20}) e^{6p_3\tau}}{\sqrt{n_{20}^2 e^{-6p_1\tau} + n_{30}^2 e^{-6p_2\tau} + e^{-6p_3\tau}}} \right],$$

$$(90d) \quad R_3 = \frac{1}{\sqrt{3}} e^{3\tau} \left[\frac{(3p_1 + 1 + \Sigma_1) n_{10} n_{20} e^{-6p_1\tau} + (3p_3 + 1 + \Sigma_3) n_{30} e^{6p_3\tau}}{\sqrt{e^{6p_1\tau} + n_{10}^2 e^{6p_2\tau} + (n_{10}n_{30} - n_{20})^2 e^{6p_3\tau}}} \right],$$

while $\Sigma_2 = -\Sigma_1 - \Sigma_3$, and where p_1, p_2, p_3 are Kasner parameters that belong to sector (321) on K° , i.e., $p_3 < p_2 < p_1$. These parameters are conveniently parametrized with \check{u} according to (18), where we recall that $\check{u} \in (-1, -\frac{1}{2})$ in sector (321). The parameter n_{20} is related to the parameters n_{10} and n_{30} according to

$$(91) \quad n_{20} = - \left[\frac{1 - \check{u}^2}{(2 + \check{u})\check{u}} \right] n_{10} n_{30}.$$

By performing a translation in τ , it is possible to scale the remaining parameters n_{10} and n_{30} and obtain expressions that only involves \check{u} and one independent parameter in the above expressions, i.e., there originates a 1-parameter set of double frame transition orbits from each Kasner point in sector (321).

A.3. The Bianchi type II subset \mathcal{B}_{II}

By setting $A_3 = 0$ in the Hamiltonian (72) (and hence $R_3 = 0$) we obtain a Hamiltonian that describes the Bianchi type II subset correctly. In this case it is beneficial to adapt

²⁸The time variable $\tau = \tau_{\text{Lim}}$ in [40] is related to the present time variable τ according to $\tau = \frac{1}{12}(w^2 + 3)\tau_{\text{Lim}}$ where the parameter w is related to \check{u} according to $w = (1 - \check{u})/(1 + \check{u})$, $\check{u} \in (-1, -\frac{1}{2})$.

the metric variables to the first direction rather than the second²⁹ which leads to

$$(92) \quad H_{\text{II}} = \frac{1}{2}(-p_0^2 + p_+^2 + p_-^2) + \frac{1}{2}A_1^2 e^{-4\sqrt{3}\beta^-} + \frac{1}{2}A_-^2 e^{4(\beta^0 - 2\beta^+)} = 0,$$

where, without loss of generality, $A_1 > 0$, and the time variable is the Taub time, t_T .

Next, following [62], we make a boost with $v = 1/2$ in the β^+ -direction in the projected diagonal minisuperspace characterized by the metric $\eta_{AB} = \text{diag}[-1, 1, 1]$ of the kinetic part of the Hamiltonian, i.e.,

$$(93) \quad (\bar{\beta}^0, \bar{\beta}^+, \bar{\beta}^-) = \left(\frac{2}{\sqrt{3}}(\beta^0 - \frac{1}{2}\beta^+), \frac{2}{\sqrt{3}}(-\frac{1}{2}\beta^0 + \beta^+), \beta^- \right).$$

This leads to the Hamiltonian

$$(94) \quad H_{\text{II}} = -\underbrace{\frac{1}{2}\bar{p}_0^2}_E + \underbrace{\frac{1}{2}\bar{p}_+^2 + \frac{1}{2}A_-^2 e^{-4\sqrt{3}\bar{\beta}^+}}_{E_+} + \underbrace{\frac{1}{2}\bar{p}_-^2 + \frac{1}{2}A_1^2 e^{-4\sqrt{3}\bar{\beta}^-}}_{E_-} = 0,$$

where E , E_{\pm} are constants thanks to that $\bar{\beta}^0$ is a cyclic coordinate and because the Hamiltonian is separable in $\bar{\beta}^+$ and $\bar{\beta}^-$. Since the E_{\pm} parts are formally the same, they result in an equivalent first order (non-linear) ODE which can be solved by making the variable transformation $x_{\pm} = e^{2\sqrt{3}\bar{\beta}^{\pm}}$. The solution is given by $\bar{\beta}^0 = -\bar{p}_0 t_T$, while

$$(95a) \quad e^{2\sqrt{3}\bar{\beta}^+} = \frac{|A_-|}{2E_+} \cosh(\sqrt{24E_+}t_T - \alpha_+),$$

$$(95b) \quad \bar{p}_+ = \sqrt{2E_+} \tanh(\sqrt{24E_+}t_T - \alpha_+),$$

$$(95c) \quad e^{2\sqrt{3}\bar{\beta}^-} = \frac{A_1}{2E_-} \cosh(\sqrt{24E_-}t_T - \alpha_-),$$

$$(95d) \quad \bar{p}_- = \sqrt{2E_-} \tanh(\sqrt{24E_-}t_T - \alpha_-).$$

To express these results in the dynamical systems setting we first introduce the variables

$$(96a) \quad \Sigma_+ = \frac{p_+}{-p_0}, \quad \Sigma_- = \frac{p_-}{-p_0},$$

$$(96b) \quad R_1 = \frac{A_1 e^{-2\sqrt{3}\beta^-}}{-p_0}, \quad N_- = \frac{A_- e^{2(\beta^0 - 2\beta^+)}}{-p_0},$$

and the time variable τ , as before defined by $d\tau/dt_T = -d\beta^0/dt_T = p_0$. Using the Misner parametrization $\Sigma_1 = -2\Sigma_+$, $\Sigma_2 = \Sigma_+ + \sqrt{3}\Sigma_-$, $\Sigma_3 = \Sigma_+ - \sqrt{3}\Sigma_-$ solves the constraint $\Sigma_1 + \Sigma_2 + \Sigma_3 = 0$, while using $\Sigma_1, \Sigma_2, \Sigma_3$ then yields the equations in (1) and (2a) for the Bianchi type II case, obtained by setting $A = N_- = 0$.

However, before translating the results in (95) into our original state space variables, it is advantageous to first introduce the following variables

$$(97a) \quad \bar{\Sigma}_+ = \frac{\bar{p}_+}{\bar{p}_0}, \quad \bar{\Sigma}_- = \frac{\bar{p}_-}{\bar{p}_0},$$

$$(97b) \quad \bar{R}_1 = \frac{A_1 e^{-2\sqrt{3}\bar{\beta}^-}}{-\bar{p}_0}, \quad \bar{N}_- = \frac{A_- e^{-2\sqrt{3}\bar{\beta}^+}}{-\bar{p}_0},$$

²⁹Thereby, using the Misner parametrization $-b_1 = \beta^0 - 2\beta^+$, $-b_2 = \beta^0 + \beta^+ + \sqrt{3}\beta^-$, $-b_3 = \beta^0 + \beta^+ - \sqrt{3}\beta^-$ in [21] and hence $\Sigma_1 = -2\Sigma_+$, $\Sigma_2 = \Sigma_+ + \sqrt{3}\Sigma_-$, $\Sigma_3 = \Sigma_+ - \sqrt{3}\Sigma_-$.

and the constants

$$(98) \quad \epsilon_{\pm} = \frac{E_{\pm}}{E} = \frac{2E_{\pm}}{\bar{p}_0^2}, \quad \bar{A}_1 = \frac{A_1}{\bar{p}_0^2}, \quad \bar{A}_- = \frac{A_-}{\bar{p}_0^2}.$$

This leads to

$$(99) \quad \epsilon_+ = \frac{2\check{u}}{1 + \check{u}^2}, \quad \epsilon_- = \frac{1 - \check{u}^2}{1 + \check{u}^2},$$

and consequently $\epsilon_+^2 + \epsilon_-^2 = 1$, where $\check{u} = \check{u}_- \in (0, 1)$ describes the past initial state (in τ) for the orbits in the original state space in sector (132), where both R_1 and N_- are unstable with respect to the past time direction τ . Hence,

$$(100a) \quad e^{2\sqrt{3}\bar{\beta}^+} = \frac{|\bar{A}_-|}{\epsilon_+} \cosh(T),$$

$$(100b) \quad \bar{\Sigma}_+ = \epsilon_+ \tanh(T),$$

$$(100c) \quad e^{2\sqrt{3}\bar{\beta}^-} = \frac{\bar{A}_1}{\epsilon_-} \cosh\left(\left(\frac{\epsilon_-}{\epsilon_+}\right)T - \alpha\right),$$

$$(100d) \quad \bar{\Sigma}_- = \epsilon_- \tanh\left(\left(\frac{\epsilon_-}{\epsilon_+}\right)T - \alpha\right),$$

where

$$(101) \quad \frac{\epsilon_-}{\epsilon_+} = \frac{1 - \check{u}^2}{2\check{u}},$$

while the time parameter $T \in (-\infty, \infty)$ is defined by³⁰ $T := 2\sqrt{3}\epsilon_+\bar{\tau}$, while $\alpha = \alpha_- - \alpha_+\epsilon_-/\epsilon_+$. Here $\alpha \in (-\infty, \infty)$ yields a 1-parameter set of orbits coming from each Kasner point characterized by $\check{u} = \check{u}_- \in (0, 1)$.

We then note that $\epsilon_+ = \epsilon_-$ implies that $\check{u} = \sqrt{2} - 1$ which corresponds to the silver ratio $u = 1 + \sqrt{2}$, see section 4.2. Moreover, at $\check{u} = \sqrt{2} - 1$ the two unstable trigger eigenvalues λ_{R_1} and λ_{N_-} are equal in sector (132). At this value of \check{u} , as for all values of \check{u} in sector (132) there originates a 1-parameter set of curvature-frame transitions. There is, however, a special orbit in this set, namely the one with $\alpha = 0$. In this case $\bar{\Sigma}_+ = \bar{\Sigma}_-$, which leads to an orbit with $\sqrt{3}\bar{\Sigma}_- = 2\bar{\Sigma}_+ - 1$ and hence $\bar{\Sigma}_1 = -2(1 - \bar{\Sigma}_3)$.

Apart from the constraint (which follows from the Hamiltonian (94) and the definitions (97)),

$$(102) \quad 1 = \bar{\Sigma}_+^2 + \bar{\Sigma}_-^2 + \bar{R}_1^2 + \bar{N}_-^2,$$

we obtain the following integral by using the hyperbolic identity

$$(103) \quad \bar{\Sigma}_+^2 + \bar{N}_-^2 = \epsilon_+^2.$$

The above formulas can be transformed into the previous variables Σ_{\pm} , R_1 and N_- by using the relations

$$(104) \quad \Sigma_+ = \frac{1 + 2\bar{\Sigma}_+}{2 + \bar{\Sigma}_+}, \quad \Sigma_- = \frac{\sqrt{3}\bar{\Sigma}_-}{2 + \bar{\Sigma}_+}, \quad R_1 = \frac{\bar{R}_1}{2 + \bar{\Sigma}_+}, \quad N_- = \frac{\sqrt{3}\bar{N}_-}{2 + \bar{\Sigma}_+}.$$

³⁰Note that $d\bar{\tau}/dt_T = -d\bar{\beta}^0/dt_T = \bar{p}_0$, and thus $\bar{\tau}$ is a time variable with the same direction as τ .

In particular, this leads to that (103) can be written as

$$(105) \quad \frac{(1 - 2\Sigma_+)^2 + 3N_-^2}{(2 - \Sigma_+)^2} = 4 \left(\frac{(1 + \Sigma_1)^2 + 3N_-^2}{(4 + \Sigma_1)^2} \right) = \epsilon_+^2.$$

Note that $\check{u} = \check{u}_- \in (0, 1)$ yields the initial (in τ , i.e., $T \rightarrow -\infty$) point for a 1-parameter set of heteroclinic orbits in sector (132) for a mixed curvature-frame transition, described by the parameter α in (100). However, the integral (105) also holds for sector (123) where $\check{u} \in (1, \infty)$ and for the point Q_1 where $\check{u} = \check{u}_- = 1$, where, in this case, the conserved quantity (105) determines the 1-parameter set of orbits.

A.4. The \mathcal{HO} subset

The \mathcal{HO} subset is obtained by setting $N_- = R_3 = \Sigma_1 = 0$ in (1). By using the same metric parametrization as in the Bianchi type II case, adapted to the first direction, and adding the potential term $\frac{1}{6}A_1^2 e^{-4\sqrt{3}\beta^-}$, corresponding to the frame rotations associated with R_1 , to the Hamiltonian for the Fermi-propagated diagonalized \mathcal{D} case in [62], leads to the following Hamiltonian:

$$(106) \quad H_D = \frac{1}{2}(-p_0^2 + p_-^2) + \frac{1}{2}A_1^2 e^{-4\sqrt{3}\beta^-} + \frac{1}{2}A_a^2 e^{4\beta^0 + 2\sqrt{3}\beta^-} = 0.$$

Introducing the variables

$$(107) \quad \Sigma_- = \frac{p_-}{-p_0}, \quad R_1^2 = A_1^2 \left(\frac{e^{-4\sqrt{3}\beta^-}}{p_0^2} \right),$$

and the usual time variable τ , leads, via the Hamiltonian equations, to the 2D dynamical system given in (33).

We recall that the system (33) has four fixed points

$$(108a) \quad \text{RT} := \left\{ (\Sigma_-, R_1) = \frac{1}{3\sqrt{3}} \left(-2, \sqrt{5} \right) \right\},$$

$$(108b) \quad \text{PW}^0 := \left\{ (\Sigma_-, R_1) = \left(-\frac{\sqrt{3}}{2}, 0 \right) \right\},$$

$$(108c) \quad \text{K}_\pm^\circ := \{ (\Sigma_-, R_1) = (\pm 1, 0) \}.$$

Linear fixed point analysis reveals the following: The fixed point RT is a local source; PW^0 is a saddle with one orbits entering the interior state space (its stable manifold is the invariant \mathcal{OT} subset $R_1 = 0$); K_+° with $(\Sigma_-, R_1) = (1, 0)$ is a saddle while K_-° with $(\Sigma_-, R_1) = (-1, 0)$ is a sink. To establish *global* results for \mathcal{HO} , we derive a monotonic function by proceeding in the same manner as for the toy model. In the present case we perform a boost in the β^- direction with $v = -2/(3\sqrt{3}) = \Sigma_-|_{\text{RT}}$ which leads to the Hamiltonian

$$(109) \quad H_D = \frac{1}{2}(-\bar{p}_0^2 + \bar{p}_-^2) + \frac{1}{2}e^{\frac{8\sqrt{3}}{23}\bar{\beta}^0} \left(A_1^2 e^{-\frac{36}{\sqrt{23}}\bar{\beta}^-} + A_a^2 e^{\frac{10}{\sqrt{23}}\bar{\beta}^-} \right) = 0.$$

We then use that the potential has a conformal exponential factor with a timelike variable with respect to the minisuperspace metric η_{AB} (i.e. $e^{\frac{8\sqrt{3}}{23}\bar{\beta}^0}$) to derive the monotonic function

$$(110) \quad M = \frac{(1 - v\Sigma_-)^2}{[R_1^5(1 - \Sigma^2)^9]^{\frac{2}{23}}},$$

which leads to

$$(111) \quad M' = \frac{27(\Sigma_- - v)^2}{23(1 - v\Sigma_-)} M.$$

Thus, M is monotonically increasing, which enables a global dynamical description of the invariant \mathcal{HO} subset, as discussed in Section 2.5.

Acknowledgments. PL was supported by Marie Skłodowska-Curie Actions, H2020 Co-fund, UNA4CAREER, 847635, with the project DynCosmos.

Competing interest and data availability. The authors have no conflict of interest to declare. Moreover, the authors confirm that the data supporting the findings of this study are available within the article.

References

- [1] L. Andersson and A. D. Rendall. Quiescent cosmological singularities. *Commun. Math. Phys.*, **218**:479, 2001.
- [2] F. Béguin. Aperiodic oscillatory asymptotic behavior for some Bianchi spacetimes. *Classical and Quantum Gravity*, **27**:185005, 2011.
- [3] F. Béguin and T. Dutilleul. Chaotic dynamics of spatially homogeneous spacetimes. *Comm. Math. Phys.*, **399**:737–927, 2023.
- [4] V. A. Belinskiĭ, I. M. Khalatnikov, and E. M. Lifshitz. A general solution of the Einstein equations with a time singularity. *Adv. Phys.*, **31**:639, 1982.
- [5] V. A. Belinskiĭ, I.M. Khalatnikov, and E. M. Lifshitz. Oscillatory approach to a singular point in the relativistic cosmology. *Adv. Phys.*, **19**:525, 1970.
- [6] P. R. Brady and J. D. Smith. Black hole singularities: A numerical approach. *Physical Review Letters*, **75**:1256, 1995.
- [7] B. Brehm. Bianchi VIII and IX vacuum cosmologies: Almost every solution forms particle horizons and converges to the Mixmaster attractor. [arXiv:1606.08058](https://arxiv.org/abs/1606.08058), 2016.
- [8] J. Buchner. *Ancient Dynamics of the Einstein Equations and the Tumbling Universe*. Dissertation, Free University of Berlin, FU-Dissertation-Server, 2013.
- [9] P. M. Chesler, R. Narayan, and E. Curiel. Singularities in reissner–nordström black holes. *Classical and Quantum Gravity*, **37**(2):025009, 2019.
- [10] K. E. M. Church, O. Hénot, P. Lappicy, J.-P. Lessard, and H. Sprink. Periodic orbits in Hořava–Lifshitz cosmologies. *General Relativity and Gravitation*, **55**(2), 2023.
- [11] M. Dafermos. Black holes without spacelike singularities. *Commun. Math. Phys.*, **332**:729–757, 2014.
- [12] T. Damour, M. Henneaux, and H. Nicolai. Cosmological billiards. *Class. Quantum Grav.*, **20**:R145, 2003.
- [13] M. Van de Moortel. The breakdown of weak null singularities inside black holes. *Duke. Math.*, **172**(15):2957–3012, 2023.

- [14] G. F. R. Ellis and M. A. H. MacCallum. A class of homogeneous cosmological models. *Commun. Math. Phys.*, **12**:108, 1969.
- [15] G. Fournodavlos, I. Rodnianski, and J. Speck. Stable big bang formation for Einstein’s equations: The complete sub-critical regime. *J. Amer. Math. Soc.*, **36**:827–916, 2023.
- [16] R. P. Geroch. Singularities in closed universes. *Physical Review Letters*, **17**:445, 1966.
- [17] H. O. Groeniger. Quiescence for the exceptional Bianchi cosmologies. [arXiv:2311.05522](https://arxiv.org/abs/2311.05522), 2023.
- [18] H. O. Groeniger, O. Petersen, and H. Ringström. Formation of quiescent big bang singularities. [arXiv:2309.11370](https://arxiv.org/abs/2309.11370), 2022.
- [19] S. W. Hawking and G. F. R. Ellis. *The Large Scale Structure of Space-Time*. Cambridge University Press, 1973.
- [20] S. W. Hawking and R. Penrose. The singularities of gravitational collapse and cosmology. *Proceedings of the Royal Society of London, Series A*, **314**:529–548, 1970.
- [21] J. M. Heinzle, N. Röhr, and C. Uggla. The cosmological billiard attractor. *Advances in Theoretical and Mathematical Physics*, **13**(2):293–407, 2009.
- [22] J. M. Heinzle and P. Sandin. The initial singularity of ultrastiff perfect fluid spacetimes without symmetries. *Commun. Math. Phys.*, **313**:385–403, 2012.
- [23] J. M. Heinzle and C. Uggla. Mixmaster: Fact and belief. *Class. Quant. Grav.*, **26**:075016, 2009.
- [24] J. M. Heinzle and C. Uggla. A new proof of the Bianchi type IX attractor theorem. *Class. Quantum Grav.*, **26**:075015, 2009.
- [25] J. M. Heinzle and C. Uggla. Monotonic functions in Bianchi models: why they exist and how to find them. *Class. Quantum Grav.*, **27**:015009, 2010.
- [26] J. M. Heinzle, C. Uggla, and W. C. Lim. Spike oscillations. *Physical Review D*, **86**(10):104049, 2012.
- [27] J. Hell, P. Lappicy, and C. Uggla. Bifurcations and chaos in Hořava-Lifshitz cosmology. *Adv. Theor. Math. Phys.*, **26**(7), 2022.
- [28] S. Hervik, R. J. van den Hoogen, W. C. Lim, and A. A. Coley. Late-time behaviour of the tilted Bianchi type VI_{-1/9} models. *Class. Quantum Grav.*, **25**:015002, 2007.
- [29] C. G. Hewitt. An investigation of the dynamical evolution of a class of Bianchi VI_{-1/9} cosmological models. *Gen. Rel. Grav.*, **23**:691–712, 1991.
- [30] C. G. Hewitt, J. T. Horwood, and J. Wainwright. Asymptotic dynamics of the exceptional Bianchi cosmologies. *Class. Quantum Grav.*, **20**:1743, 2003.
- [31] C. G. Hewitt and J. Wainwright. A Dynamical systems approach to Bianchi cosmologies: Orthogonal models of class B. *Class. Quant. Grav.*, **10**:99–124, 1993.
- [32] S. Hod and T. Piran. Mass inflation in dynamical gravitational collapse of a charged scalar field. *Physical Review Letters*, **81**:1554, 1998.

- [33] R. T. Jantzen. *Spatially Homogeneous Dynamics: A Unified Picture*. Proc. Int. Sch. Phys. “E. Fermi” Course LXXXVI on “Gamov Cosmology”, R. Ruffini, F. Melchiorri, Eds. (North Holland, Amsterdam, 1987) and in *Cosmology of the Early Universe*, R. Ruffini, L.Z. Fang, Eds. World Scientific, Singapore, 1984, 1984.
- [34] I. M. Khalatnikov, E. M. Lifshitz, K. M. Khanin, L. N. Shur, and Y. G. Sinai. On the stochasticity in relativistic cosmology. *J. Stat. Phys.*, **38**:97, 1985.
- [35] D. Simmons L. Fishman and M. Urbański. Diophantine properties of measures invariant with respect to the Gauss map. *J. d’Analyse Mathématique*, **122**:289–315, 2014.
- [36] P. Lappicy and V. H. Daniel. Chaos in spatially homogeneous Hořava–Lifshitz sub-critical cosmologies. *Classical and Quantum Gravity*, **39**(13):135017, 2022.
- [37] S. Liebscher, J. Harterich, K. Webster, and M. Georgi. Ancient dynamics in Bianchi models: Approach to periodic cycles. *Comm. Math. Phys.*, **305**:59–83, 2011.
- [38] S. Liebscher, A. Rendall, and S. B. Tchapnda. Oscillatory singularities in Bianchi models with magnetic fields. *Ann. Henri Poincaré*, **14**:1043–1075, 2013.
- [39] E. M. Lifshitz and I.M. Khalatnikov. Investigations in relativistic cosmology. *Adv. Phys.*, **12**:185, 1963.
- [40] W. C. Lim. Non-orthogonally transitive G2 spike solution. *Classical and Quantum Gravity*, **32**:162001, 2015.
- [41] W. C. Lim. Numerical confirmations of joint spike transitions in G2 cosmologies. *Class. Quant. Grav.*, **39**(6):065001, 2022.
- [42] W. C. Lim and M. Z. A. Moughal. Transition analysis of the non-OT G2 stiff fluid spike solution. *Classical and Quantum Gravity*, **39**(2):025010, 2021.
- [43] W.C. Lim, C. Uggla, and J. Wainwright. Asymptotic silence-breaking singularities. *Class. Quant. Grav.*, **23**:2607, 2006.
- [44] J. Luk. Weak null singularities in general relativity. *J. Amer. Math. Soc.*, **31**(1):1–63, 2018.
- [45] J. Luk. *Singularities in general relativity*. Proc. International Congress of Mathematicians (D.Beliaev and S. Smirnov, eds.), ICM 2022, Volume 5, Sections 9–11. Berlin: European Mathematical Society (EMS), 2023.
- [46] C. W. Misner. Mixmaster universe. *Phys. Rev. Lett.*, **22**:1071, 1969.
- [47] A. Nützi, M. Reiterer, and E. Trubowitz. Semiglobal non-oscillatory big bang singular spacetimes for the Einstein-scalar field system. [arXiv:2005.03395](https://arxiv.org/abs/2005.03395), 2020.
- [48] A. Ori and É. É. Flanagan. How generic are null spacetime singularities? *Phys. Rev. D*, **53**:R1754(R), 1996.
- [49] R. Penrose. Gravitational collapse and space-time singularities. *Physical Review Letters*, **14**:57–59, 1965.
- [50] M. Reiterer and E. Trubowitz. The BKL conjectures for spatially homogeneous spacetimes. [arXiv:1005.4908](https://arxiv.org/abs/1005.4908), 2010.

- [51] A. Rendall. *The nature of spacetime singularities*. In Ashtekar, A.: 100 years of relativity. Spacetime structure: Einstein and beyond. World Scientific, Singapore., 2005.
- [52] H. Ringström. Curvature blow up in Bianchi VIII and IX vacuum spacetimes. *Class. Quantum Grav.*, **17**:713, 2000.
- [53] H. Ringström. The Bianchi IX attractor. *Annales Henri Poincaré*, **2**:405, 2001.
- [54] I. Rodnianski and J. Speck. A regime of linear stability for the Einstein-scalar field system with applications to nonlinear big bang formation. *Ann. of Math.*, **187**(1):65–156, 2012.
- [55] N. Röhr and C. Uggla. Conformal regularization of Einstein’s field equations. *Class. Quant. Grav.*, **22**:3775, 2005.
- [56] W. Schmidt. Badly approximable systems of linear forms. *J. Number Theory*, **1**:139–154, 1969.
- [57] W. Schmidt. *Diophantine Approximation*. Lecture Notes in Mathematics, 785. Springer, Berlin, 1980.
- [58] J. M. M. Senovilla and D. Garfinkle. The 1965 Penrose singularity theorem. *Classical and Quantum Gravity*, **32**(12):124008, 2015.
- [59] H. Stephani, D. Kramer, M. MacCallum, C. Hoenselaers, and E. Herlt. *Exact Solutions of Einstein’s Field Equations*. Cambridge University Press, 2 edition, 2003.
- [60] C. Uggla. Recent developments concerning generic spacelike singularities. *Gen. Rel. Grav.*, **45**:1669–1710, 2013.
- [61] C. Uggla. Spacetime singularities: Recent developments. *Int. J. Mod. Phys. D*, **22**:1330002, 2013.
- [62] C. Uggla, R. T. Jantzen, and K. Rosquist. Exact hypersurface-homogeneous solutions in cosmology and astrophysics. *Phys. Rev. D*, **51**:5522, 1995.
- [63] J. Wainwright and G. F. R. Ellis. *Dynamical systems in cosmology*. Cambridge University Press, 1997.